doi:10.1510/icvts.2009.219006

INTERACTIVE CARDIOVASCULAR AND THORACIC SURGERY

Interactive CardioVascular and Thoracic Surgery 10 (2010) 356-359

www.icvts.org

Work in progress report - Experimental

Granulation tissue formation at the bronchial stump is reduced after stapler closure in comparison to suture closure in dogs☆

Yotaro Izumi[a,*], Masafumi Kawamura[a], Masatoshi Gika[b], Hiroaki Nomori[a]

[a]Division of General Thoracic Surgery, Department of Surgery, School of Medicine Keio University, 35 Shinanomachi, Shinjuku-ku, Tokyo 160-8582, Japan
[b]Department of Thoracic Surgery, Saitama Medical Center, Saitama Medical School, Saitama, Japan

Received 13 August 2009; received in revised form 17 November 2009; accepted 19 November 2009

Abstract

The aim of this study was to compare the morphology of the bronchial stump after lobectomy between mechanical stapler closure and manual suture closure. The effect of fibrin glue application on each method of closure was also observed. Right upper lobectomy was performed in beagles ($n=31$) using staplers (ST group) or sutures (SU group). In a separate experiment, fibrin glue was sprayed onto the stump after each respective method of closure. After one week, the stump region was examined macroscopically, and also by histology. χ^2-Test and Mann–Whitney test were used for comparative analysis. The incidence of adhesion formation between the surrounding tissues was significantly reduced in the ST group in comparison to the SU group (22 vs. 80%, $P=0.04$). The thickness of granulation tissue over the stump was significantly reduced in the ST group in comparison to the SU group (0.8 ± 0.2 vs. 2.5 ± 0.3 mm, $P<0.0001$). Vessel density in the granulation tissue was also significantly reduced in the ST group in comparison to the SU group (6 ± 2 vs. 16 ± 2, $P=0.003$). Fibrin glue application after stapler closure significantly increased the incidence of adhesion formation, granulation tissue thickness, and vessel density in the granulation tissue over the stump.

Keywords: Granulation tissue; Bronchial stump; Lung lobectomy

1. Introduction

Previous studies in animals have demonstrated that the sutured bronchial stump heals primarily through secondary closure. Therefore, it is speculated that the level of attachment between the stump and surrounding tissues, and the magnitude of granulation tissue formation at the bronchial stump, should be important factors in stump healing or broncho-pleural fistula (BPF) formation [1]. Several retrospective clinical studies have shown that the incidence of BPF formation is similar between mechanical stapling and manual suturing [2–4]. However, there are some studies which suggest that once BPF is initiated, the magnitude of stump dehiscence may be greater with mechanical stapling [5, 6]. To this end, there may be differences in the bronchial stump healing between stapler and manual suture closure [7], but the morphological aspects have not been examined in detail. In the present study, we examined the bronchial stump one week after right upper lobectomy in dogs, and compared the morphology between stapler and manual suture closure.

A number of reports suggest that granulation tissue formation is facilitated by local application of fibrin glue [8–12], although the exact mechanisms remain unclear. To our knowledge, there is one report on the effect of fibrin glue application to the bronchial stump after suture closure [13]. In this report, significant thickening of the tissue in the vicinity of the stump after fibrin glue application is documented, but the actual morphological changes are not specifically described. Therefore, we also observed the effect of fibrin glue application on the bronchial stump after stapler or suture closure.

2. Materials and methods

2.1. Animal experiment

Female beagles aged 5–7 months, weighing 8–10 kg (Kitayama Labs Co, Ltd, Nagano, Japan) ($n=31$) were used for the study. After induction of general anesthesia, the animal was mechanically ventilated with 40% oxygen. Tidal volume was ~200 ml, and respiratory rate was 14 per minute.

Right 4th intercostal thoracotomy was performed. The pulmonary arteries, and veins of the right upper lobe were ligated by silk strings and dissected. The connective tissue around the right upper bronchus was bluntly dissected, and the bronchial arteries of the right upper lobe bronchus were ligated and dissected. In the stapler closure (ST) group ($n=9$), Endopath ETS Compact Flex-45, blue cartridge (3.5 mm thickness), (Ethicon Endo-Surgery LLC, USA) was used and the right upper lobe bronchus was stapled and cut similar to Sweet's method. In the manual suture

☆ This study was supported in part by grant in aid from the Ministry of Education, Culture, Sports, Science and Technology, Japan (19591645) to Y.I.

*Corresponding author. Tel.: +813-5363-3806; fax: +813-5363-3499.
E-mail address: yotaroizumi@a2.keio.jp (Y. Izumi).

closure (SU) group ($n=5$), the right upper lobe bronchus was cut with a scalpel ~5 mm from the bifurcation. The stump was manually sutured using Sweet's method, with 4-0 PDS II (Ethicon Inc, USA) interrupted sutures, ~2 mm apart. The length of the stump was similar in both groups at closure. In the fibrin glue application groups, 1 ml each of liquid fibrinogen, and liquid thrombin (Bolheal, Chemo-Sero-Therapeutic Research Institute, Kumamoto, Japan), were sprayed together onto the stump after either stapler closure (STGL group, $n=9$), or manual suture closure (SUGL group, $n=5$). In all experiments, the stump was tested for the absence of air leakage up to 40 cm H_2O of airway pressure and the chest was closed. A similar experiment was also performed using 2.5 mm thickness staplers, ($n=3$), Endopath ETS Compact Flex-45, white cartridge (2.5 mm thickness), (Ethicon Endo-Surgery LLC, USA).

After one week, the right upper lobe stump region was carefully examined, and the presence/absence of adhesion between the surrounding tissues was documented. The animals were sacrificed and the right upper lobe stump region was resected together with the surrounding tissue when adhesion was present.

All animal studies were approved by the School of Medicine, Keio University Institutional Animal Care and Use Committee, and complied with the European Convention on Animal Care.

2.2. Histological examinations

The resected specimens were fixed in 10% formalin. Cross-sections of the bronchial stumps were made perpendicular to the line of closure. The location and orientation of each stump was verified from the lumen of the right main bronchus before sectioning. Three sections were made per stump. Staples were carefully removed under a magnifying glass before section preparation in the ST and STGL groups. The sections were embedded in paraffin, and three micron sections were made. The sections were stained with haematoxylin and eosin for morphological examinations. The minimum distance between the bronchial epithelium lining the inner lumen of the stump and the edge of the granulation tissue covering the stump was measured as stump granulation tissue thickness for each section. This was done using Image J by drawing a circle encompassing the stump bronchial epithelial lining and the closest outer edge of the granulation tissue, and measuring its diameter. The thickness of the fibrin glue, or any adhered tissue was excluded. The measurements from three sections were averaged per animal.

Immunohistochemistry using anti-factor VIII antibody (1/2000 anti-human factor VIII (Dako A0082)) was done for vessel staining. The number of vessels were counted as vessel density under 400× magnification in five randomly chosen fields for each section within the granulation tissue covering the stump. The measurements from three sections were averaged per animal.

The slides were masked for analyses, but the presence of fibrin glue and/or fragments of sutures precluded complete masking.

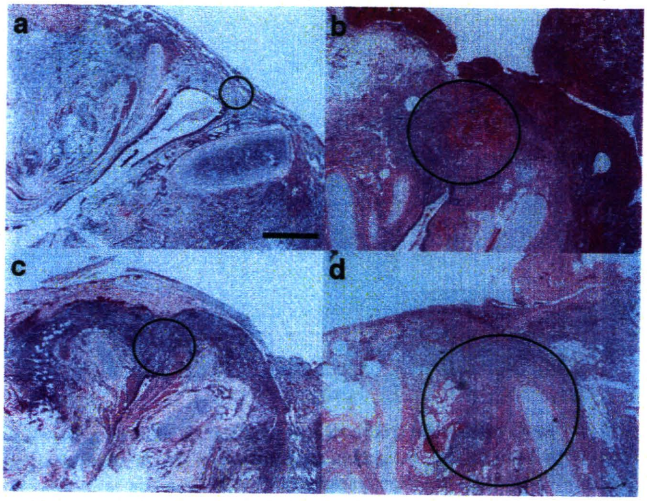

Fig. 1. The appearances of the right upper lobe stump seven days after lobectomy are shown using mechanical staplers (a), manual sutures (b), mechanical staplers and fibrin glue (c), or manual sutures and fibrin glue (d). Stump granulation thickness was measured as in the methods. Haematoxylin and eosin staining. Scale bar indicates 1 mm.

2.3. Data analysis

Data are shown as mean±standard deviation (S.D.). The rates of adhesion formation were compared between groups using χ^2-test (StatView, SAS Institute Inc, Cary, NC). Other comparisons were made between groups using Mann–Whitney U-test (StatView, SAS Institute Inc, Cary, NC). Significance was assumed at $P<0.05$.

3. Results

All the animals survived. There were no apparent abnormalities in behavior or feeding in any of the animals. At one-week, re-thoracotomy revealed no apparent indications of delayed bleeding or infection in any of the animals. The presence of adhesion at the stump in the ST, STGL, SU, and SUGL groups were 22%, 77%, 80%, and 60%, respectively. The adhesions were seen between the stump and the lung and/or the azygous vein. The incidences of adhesion formation were statistically different between the ST and STGL groups ($P=0.02$), and the ST and SU groups ($P=0.04$).

Histologically, there was no apparent indication of excessive inflammatory reactions at the stump in any of the groups. The bronchial cartilages at the stump were satisfactorily aligned, with no indications of damage in any of the groups. The luminal side of the bronchial stump was lined by bronchial epithelium in all groups. The magnitude of granulation tissue formation at the stump was different between groups (Fig. 1a–d). Stump granulation tissue thickness, measured as in the methods, was significantly reduced in the ST group in comparison to the SU group (ST vs. SU, $P<0.0001$). Application of fibrin glue significantly increased stump granulation thickness in the STGL group in comparison to the ST group (ST vs. STGL, $P<0.0001$), but not to the extent of the SU group (STGL vs. SU, $P=0.004$). There was no statistical difference in stump granulation thickness between the SU group and SUGL group (SU vs. SUGL, $P=0.13$) (Fig. 2). The vessel density within the

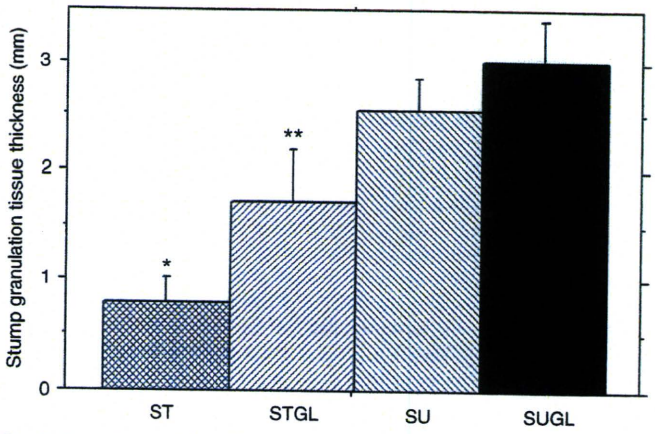

Fig. 2. Stump granulation thickness was significantly reduced in the ST group in comparison to the SU group. Application of fibrin glue significantly increased stump granulation thickness in the STGL group in comparison to the ST group, but not to the extent of the SU group. *$P<0.05$ ST group vs. all other groups, **$P<0.05$ STGL group vs. SU group and SUGL group. ST, stapler closure; SU, suture closure; STGL, stapler closure plus fibrin glue; SUGL, suture closure plus fibrin glue.

stump granulation tissue was also significantly reduced in the ST group in comparison to the SU group (ST vs. SU, $P=0.003$). Application of fibrin glue significantly increased vessel density in the STGL group in comparison to the ST group (ST vs. STGL, $P=0.001$), and there was no statistical difference between the STGL group and the SU group (STGL vs. SU, $P=0.13$). There was no statistical difference in vessel density between the SU group and SUGL group (SU vs. SUGL, $P=0.06$) (Fig. 3).

In the 2.5 mm thickness stapler group, although there was no apparent development of BPF at one-week, there was only minimal granulation tissue formation over the bronchial stump. Furthermore, the luminal side of the bronchial stump was only sparsely lined with bronchial epithelium at the distal end of the stump, and, therefore, the stump granulation tissue thickness, as defined in this particular study, could not be measured (Fig. 4). The vessel density also could not be adequately evaluated due to the limited amount of granulation tissue covering the stump.

4. Discussion

The findings of the present study indicate that adhesion formation as well as granulation tissue formation is significantly reduced at the bronchial stump after stapler closure in comparison to suture closure. This may at least in part be due to the reduction in tissue perfusion as suggested by the significant decrease in vessel density in the granulation tissue over the stapled stump. This tendency was more prominent with the use of a thinner stapler, and, therefore, tissue compression by the staples is suggested to be one of the predominant causes of these findings. Another possible cause may be the additional induction of initial inflammatory responses due to stump manipulation during suturing in the SU group, in comparison to stapler closure in ST group, in which the stump was closed and swiftly cut.

In the present study, we measured the minimum distance between the stump lumen and the edge of the granulation tissue covering the stump in each section, because at least morphologically, it seemed to be acceptable to assume that the probability of BPF would be related to this distance. Intuitively, we feel that stump granulation tissue thickness, along with the presence or absence of adhesion, may at least in part, correlate with the incidence and/or magnitude of BPF. But the actual relevance of stump morphology to the risk of BPF formation is only speculative, including the possibility that BPF may occur through different processes in stapler vs. suture closure. Additionally, since the reported incidence of clinical BPF is similar between stapler closure and suture closure, the findings in this study do not translate directly to increased BPF formation in the clinical setting. This implies that other mechanisms may contribute

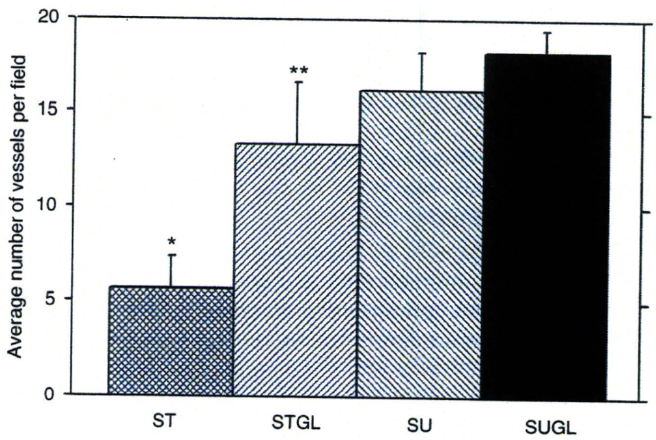

Fig. 3. The average number of vessels per field (vessel density) within the stump granulation tissue was significantly reduced in the ST group in comparison to the SU group. Application of fibrin glue significantly increased vessel density in the STGL group in comparison to the ST group, and there was no statistical difference between the STGL group and the SU group. *$P<0.05$ ST group vs. all other groups, **$P=0.02$ STGL group vs. SUGL group. ST, stapler closure; SU, suture closure; STGL, stapler closure plus fibrin glue; SUGL, suture closure plus fibrin glue.

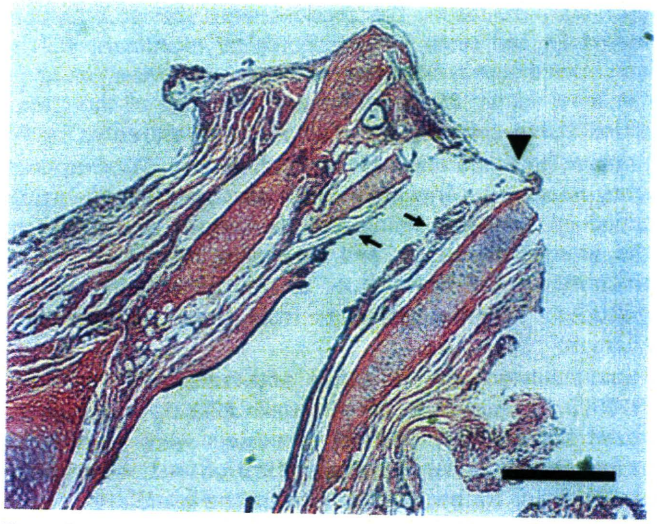

Fig. 4. The appearance of the right upper lobe stump seven days after lobectomy using a 2.5-mm thickness mechanical stapler. There was only minimal granulation tissue formation over the bronchial stump (arrowhead), and the lumen of the bronchial stump was only sparsely lined with bronchial epithelium at the distal end of the stump (arrows). Haematoxylin and eosin staining. Scale bar indicates 1 mm.

to bronchial stump healing, or that the amount of granulation tissue formation in the ST group is sufficient to maintain stump closure. But still, the results of this study prompt us to consider reinforcement of the stapled stump with sutures or materials, such as muscle flaps, particularly if the staples appear to be constricting the stump after closure. Testing the strength of the stump by pressure measurements may provide additional evidence, but an animal model in which clinically relevant BPF can be reproducibly induced is necessary to further investigate these speculations.

In the present study, local application of fibrin glue over the stump increased the incidence of adhesion formation, particularly in the stapler closure groups. Fibrin glue application also increased granulation tissue thickness over the stump, and vessel density within the granulation tissue, particularly in the stapler closure groups. Fibrin glue seems to facilitate wound healing in a number of experimental reports, at least in part by providing a suitable framework for the development of granulation tissue along with augmented cell migration and angiogenesis [8–12]. On the other hand, whether fibrin glue prevents or facilitates adhesion formation is still controversial [12, 14, 15]. These studies were conducted each under different experimental conditions, and so the effect is probably context dependent. In this particular study, fibrin glue application seems to have augmented adhesion formation in the stapler closure groups, but this tendency was not apparent in the suture closure groups. The results of the present study suggest that local application of fibrin glue may augment granulation tissue formation at the bronchial stump.

The onset of BPF was reported to range from 5 to 16 days after surgery [2, 4], and, therefore, we examined the bronchial stump at seven days after surgery. But studies with longer observation periods will be necessary to see if granulation tissue formation at the stump is actually reduced or just delayed after stapler closure in comparison to suture closure. The fate of the applied fibrin glue also needs to be observed for longer periods. Studies looking at the stump after more extensive bronchial artery dissection, or after interventions, such as chemotherapy or radiation, are also necessary as more clinically relevant models of BPF formation.

Acknowledgements

We thank the scientists at The Chemo-Sero-Therapeutic Research Institute (KAKETSUKEN), Noriko Shinya and Satomi Tomita, Pathology Department, and Sumika Miyabashira, Therapeutic Protein Products Research Department, for their expertise in animal experiments and histology analyses, and Kentaro Yano, Research Department 1, for his expertise in fibrin glue preparation.

References

[1] Rienhoff WF, Gannon J, Sherman I. Closure of the bronchus following total pneumonectomy. Ann Surg 1942;116:481–531.
[2] Vester SR, Faber LP, Kittle CF, Warren WH, Jensik RJ. Bronchopleural fistula after stapled closure of bronchus. Ann Thorac Surg 1991;52: 1253–1257.
[3] Sonobe M, Nakagawa M, Ichinose M, Ikegami N, Nagasawa M, Shindo T. Analysis of risk factors in bronchopleural fistula after pulmonary resection for primary lung cancer. Eur J Cardiothorac Surg 2000;18:519–523.
[4] Asamura H, Kondo H, Tsuchiya R. Management of the bronchial stump in pulmonary resections: a review of 533 consecutive recent bronchial closures. Eur J Cardiothorac Surg 2000;17:106–110.
[5] Takizawa T, Terashima M, Koike T, Akamatsu H. Selection of staple for closure of the lobar bronchus. Nippon Kyobu Geka Gakkai Zasshi 1996; 44:1717–1720.
[6] Takizawa T, Koike T, Aoki T. Development of bronchopleural fistula in relation to the method of bronchial closure. Kikanshigaku 1997;19:211–214.
[7] Salci H, Bayram AS, Ozyigit O, Gebitekin C, Gorgul OS. Comparison of different bronchial closure techniques following pneumonectomy in dogs. J Vet Sci 2007;8:393–399.
[8] Takagi M, Akiba T, Yamazaki Y, Nariai K, Iwaki T. The wound-healing effect of fibrin glue for tracheal anastomosis in experimental pulmonary surgery. Surg Today 2001;31:845–847.
[9] Kanellos I, Mantzoros I, Demetriades H, Kalfadis S, Kelpis T, Sakkas L, Betsis D. Healing of colon anastomoses covered with fibrin glue after immediate postoperative intraperitoneal administration of 5-fluorouracil. Dis Colon Rectum 2004;47:510–515.
[10] Kanellos D, Blouhos K, Pramateftakis MG, Kanellos I, Demetriades H, Sakkas L, Betsis D. Effect of 5-fluorouracil plus interferon on the integrity of colonic anastomoses covering with fibrin glue. World J Surg 2007;31:186–191.
[11] Kroez M, Lang W, Dickneite G. Wound healing and degradation of the fibrin sealant Beriplast P following partial liver resection in rabbits. Wound Repair Regen 2005;13:318–323.
[12] van der Ham AC, Kort WJ, Weijma IM, van den Ingh HF, Jeekel J. Effect of fibrin sealant on the healing colonic anastomosis in the rat. Br J Surg 1991;78:49–53.
[13] Takagi M, Akiba T. Wound healing effect of fibrin adhesive agent in bronchial stump after pulmonary lobectomy. Tokyo Jikeikai Medical Journal 1996;111:145–154.
[14] de Virgilio C, Elbassir M, Hidalgo A, Schaber B, French S, Amin S, Stabile BE. Fibrin glue reduces the severity of intra-abdominal adhesions in a rat model. Am J Surg 1999;178:577–580.
[15] Petter-Puchner AH, Walder N, Redl H, Schwab R, Ohlinger W, Gruber-Blum S, Fortelny RH. Fibrin sealant (Tissucol) enhances tissue integration of condensed polytetrafluoroethylene meshes and reduces early adhesion formation in experimental intraabdominal peritoneal onlay mesh repair. J Surg Res 2008;150:190–195.

AUGUST 2009
Volume 20, Number 8

Bioconjugate Chemistry

REVIEWS

Artificial Oxygen Carriers, Hemoglobin Vesicles and Albumin−Hemes, Based on Bioconjugate Chemistry

Eishun Tsuchida,*[,†] Keitaro Sou,[†] Akito Nakagawa,[†] Hiromi Sakai,[†] Teruyuki Komatsu,[†,‡] and Koichi Kobayashi[§]

Research Institute for Science and Engineering, Waseda University, Tokyo 169-8555, Japan, PRESTO, Japan Science and Technology Agency (JST), and Department of General Thoracic Surgery, School of Medicine, Keio University, Tokyo 160-8582, Japan. Received October 10, 2008; Revised Manuscript Received December 10, 2008

Hemoglobin (Hb, Mw: 64 500) and albumin (Mw: 66 500) are major protein components in our circulatory system. On the basis of bioconjugate chemistry of these proteins, we have synthesized artificial O_2 carriers of two types, which will be useful as transfusion alternatives in clinical situations. Along with sufficient O_2 transporting capability, they show no pathogen, no blood type antigen, biocompatibility, stability, capability for long-term storage, and prompt degradation in vivo. Herein, we present the latest results from our research on these artificial O_2 carriers, Hb-vesicles (HbV) and albumin−hemes. (i) HbV is a cellular type Hb-based O_2 carrier. Phospholipid vesicles (liposomes, 250 nm diameter) encapsulate highly purified and concentrated human Hb (35 g/dL) to mimic the red blood cell (RBC) structure and eliminate side effects of molecular Hb such as vasoconstriction. The particle surface is modified with PEG-conjugated phospholipids, thereby improving blood compatibility and dispersion stability. Manipulation of physicochemical parameters of HbV, such as O_2 binding affinity and suspension rheology, supports the use of HbV for versatile medical applications. (ii) Human serum albumin (HSA) incorporates synthetic Fe^{2+} porphyrin (FeP) to yield unique albumin-based O_2 carriers. Changing the chemical structure of incorporated FeP controls O_2 binding parameters. In fact, PEG-modified HSA-FeP showed good blood compatibility and O_2 transport in vivo. Furthermore, the genetically engineered heme pocket in HSA can confer O_2 binding ability to the incorporated natural Fe^{2+} protoporphyrin IX (heme). The O_2 binding affinity of the recombinant HSA (rHSA)-heme is adjusted to a similar value to that of RBC through optimization of the amino acid residues around the coordinated O_2.

1. INTRODUCTION

Transfusion of donor blood is currently an indispensable routine procedure in modern medical treatments because the risk of transmission of viral illness has became extremely low. Nevertheless, this level of safety has been achieved at great cost and hepatitis virus or unknown pathogens cannot be excluded completely, even by the nucleic acid amplification test (NAT) system. Furthermore, the transfusion of donor blood necessitates cross matching and compatibility tests to avoid a hemolytic reaction in the recipient, and the donated red blood cells (RBCs) must be refrigerated at 4 °C (up to 3 weeks in Japan). These requirements limit the availability of blood transfusion in disaster or emergency situations.

* To whom correspondence should be addressed. Eishun Tsuchida, Ph.D. Phone: −81-3-5286-3120. Fax: −81-3-3205-4740. E-mail: eishun@waseda.jp.
† Waseda University.
‡ JST.
§ Keio University.

10.1021/bc800431d CCC: $40.75
Published on Web 02/10/2009

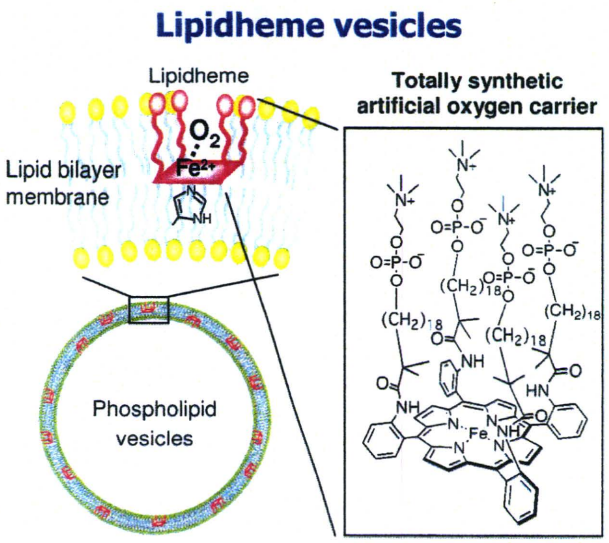

Figure 1. Lipidheme phospholipid vesicles as a totally synthetic artificial O_2 carrier (*7*).

During the past several decades, various artificial O_2 carriers have been synthesized and studied for as RBC substitutes by many scientists in the fields of organic chemistry, inorganic chemistry, biochemistry, and polymer chemistry. These O_2 carriers are classified as perfluorocarbon-based materials, synthetic Fe^{2+}porphyrin-based materials, and Hb-based materials. In this review, we highlight recent developments of our research related to RBC substitutes of the latter two types.

Actually, Hb consists of four polypeptide chains (globin proteins), each of which has an Fe^{2+}protoporphyrin IX (heme) as a prosthetic group. The globin chain forms a compact globular conformation; the heme group is incorporated into the hydrophobic pocket with an axial coordination of histidine (*1*). On exposure of the Hb solution to O_2, the heme forms a stable O_2 adduct complex. However, if the heme is eliminated from the globin wrapping, the heme complex is oxidized immediately and irreversibly to its Fe^{3+} state by proton-driven oxidation or μ-oxo dimer formation (*2*). In the 1970s and 1980s, much research was directed to mimic the O_2 carrier by synthesizing substituted porphyrin derivatives. In aprotic solvents, the proton-driven oxidation is excluded completely. Therefore, the remaining problem is how to suppress irreversible oxidation via dimerization. One successful approach was steric modification of porphyrin. Some superstructured Fe^{2+}porphyrins were prepared using an elegant organic synthesis technique (*2*−*4*). In particular, Collman reported that the tetrakis(α,α,α,α-*o*-pivalamido)phenylporphinatoiron complex with 1-methylimidazole can reversibly bind O_2 in benzene at room temperature (*5*, *6*). Nevertheless, these synthetic porphyrins were all oxidized irreversibly in aqueous media.

To create a hydrophobic environment in water, it is possible to use a bilayer membrane of a phospholipid vesicle instead of globin protein. In 1983, we synthesized an amphiphilic Fe^{2+}porphyrin having four alkylphosphocholine groups (lipidheme), which is efficiently embedded into the bilayer of the phospholipid vesicle to yield a homogeneous hybrid. This lipidheme/phospholipid vesicle can bind and release O_2 under physiological conditions (Figure 1) (*7*−*9*). The 10 mM lipidheme/phospholipid vesicle solution dissolves 29 mL O_2/dL compared to 27 mL/dL of human blood. Subsequent to that finding, we synthesized over 60 lipidheme molecules. A new lipidheme having four dialkyl-*sn*-glycerophosphocholine groups is self-organized in water to form self-assembled porphyrin bilayer vesicles without phospholipid (*10*). Furthermore, in 1995, we found that synthetic Fe^{2+} porphyrin bearing a covalently linked proximal base (FeP**1**) is incorporated into human serum albumin (HSA) and the obtained HSA-FeP**1** hybrid coordinates O_2 in aqueous medium (*11*).

In 1985, we began the study of Hb-based O_2 carriers using purified human Hb aiming at the beneficial utilization of outdated RBC to support the present blood donation−transfusion system. This project has been supported for a long time by Japanese Red Cross Society and Ministry of Health and Welfare, Japan. On the basis of a fundamental concept that the cellular structure of RBC is necessary for O_2 transport in the bloodstream, we designed the phospholipid vesicle encapsulating Hb: the so-called Hb-vesicle. It has to be emphasized that the Hb-vesicle comprises a concentrated Hb solution and four kinds of natural and synthetic lipids that assemble to form a hierarchical corpuscle structure (molecular assembly) through the well-regulated secondary interactions, such as hydrophobic and electrostatic interactions. To date, chemically modified Hb of several types have been developed as RBC substitutes or O_2 therapeutic reagents. Herein, we review the latest developments of our research into Hb-vesicles and albumin−hemes.

2. HEMOGLOBIN VESICLES THAT MIMIC THE RBC CELLULAR STRUCTURE

2.1. Physiological Importance of Cellular Structure of RBC for Encapsulated Hb Design. Historically, stroma-free Hb isolated from RBCs were tested as a principal material for carrying O_2. However, the plasma retention time of stroma-free Hb is particularly short (half-life of 0.5−1.5 h) because of the dissociation of the Hb tetramer ($\alpha_2\beta_2$; Mw, 64 500; 6.5 nm diameter) into dimers ($2\alpha\beta$), which are subsequently filtered by the kidney (*12*). Cell-free Hb-based O_2 carriers have been developed to overcome the problems of stroma-free Hb through chemical modification, "bioconjugation", of Hb molecules (Figure 2). They include intramolecularly cross-linked Hb (DCLHb) to prevent dimerization, recombinant cross-linked Hb produced by *E. coli*, polymerized Hb using glutaraldehyde or other cross-linkers, and polymer-conjugated Hb such as PEG-conjugated Hb and polysaccharide-conjugated Hb (*13*−*21*). During the long history of the development of cell-free Hb-based O_2 carriers (HBOCs), the many side effects of stroma-free Hb and chemically modified Hbs have been well-documented: renal toxicity; entrapment of gaseous messenger molecules (NO and CO) inducing vasoconstriction, hypertension, reduced blood flow, and reduced tissue oxygenation at microcirculatory levels (*22*−*25*); neurological disturbances; malfunction of esophageal motor function (*18*); myocardial lesions (*26*, *27*); and death (*28*). These side effects of Hb molecules underscore the importance of the large dimension of HBOCs or the RBC cellular structure. Retrospective and recent observations have indicated the main justifications for Hb encapsulation in RBCs: (i) a decreased high colloidal osmotic pressure (*15*); (ii) prevention of the removal of Hb from blood circulation; (iii) prevention of direct contact of toxic Hb molecules and the endothelial lining (*29*); (iv) retardation of reactions with endogenous NO and CO (*24*, *25*, *30*, *31*) (Figure 3); (v) preservation of the chemical environment in cells, such as the concentration of phosphates (2,3-DPG, ATP, etc.) and other electrolytes; (vi) RBCs are the major component that renders blood as non-Newtonian and viscous, which is necessary to pressurize the peripheral artery for homogeneous blood distribution and for maintenance of blood circulation (*32*); (vii) the RBC cellular structure retards O_2-release in comparison to acellular Hb solutions (*33*, *34*), thereby retaining O_2 to peripheral tissues where O_2 is required. For those reasons, the optimal structure of Hb-based O_2 carriers might be to mimic the RBC cellular structure.

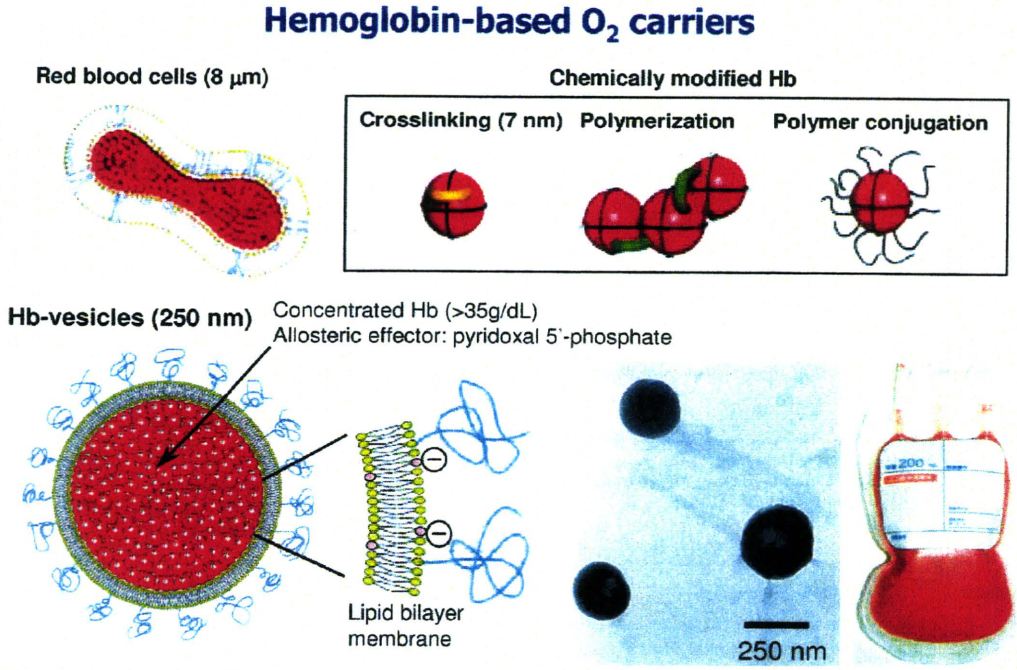

Figure 2. Schematic representation of a series of Hb-based O_2 carriers. Cross-linked Hb, polymerized Hb, and polymer-conjugated Hb are based on the chemical modification of Hb molecules (chemically modified Hbs). In the case of Hb-vesicles, a purified and concentrated Hb solution (35 g/dL) is encapsulated in phospholipid vesicles and the surface is modified using PEG chains. The particle size is well-regulated at 250 nm.

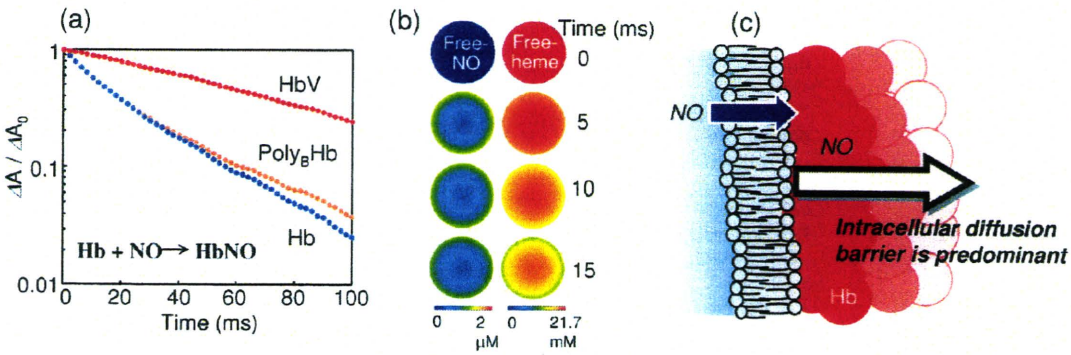

Figure 3. Encapsulation of Hb in vesicles retards NO binding. (a) Time courses of NO binding with HbV, human Hb with PLP (Hb/PLP = 1:2.5 by mol), and polymerized bovine Hb ($Poly_BHb$) observed by stopped-flow rapid scan spectrophotometry. The level of reaction was plotted on a semilogarithmic graph as a ratio of absorption at 430 nm (ΔA) at time t, to the initial absorption (ΔA_0) at time 0. NO-bubbled PBS ([NO] = 3.8 μM) and deoxygenated-Hb-containing solutions in PBS ([heme] = 3.0 μM) were mixed (*31*). (b) Schematic two-dimensional representation of the simulated time courses of distributions of unbound free NO and unbound free heme in one HbV (250 nm). Both free NO and unbound hemes are distributed heterogeneously. The concentration changes gradually from the surface to the core, indicating formation of the intracellular diffusion barrier (*30*). (c) The phospholipid bilayer membrane cannot have any barrier function to gas diffusion. The determinant factor of retardation of NO-binding should be the intracellular diffusion barrier, which was induced by (i) intrinsically larger binding rate constant of NO to a heme in an Hb molecule, (ii) numerous hemes as sites of gas entrapment at a higher Hb concentration, (iii) a slowed gas diffusion in the intracellular viscous Hb solution, and (iv) a longer gas diffusion distance in a larger capsule.

In 1957, Chang performed the pioneering work of Hb encapsulation to mimic the cellular structure of RBCs (*35*); microcapsules (5 μm) were prepared using nylon, collodion, and other materials. Toyoda in 1965 (*36*) and the Kambara–Kimoto group in 1968 (*37*) also investigated encapsulation of Hbs with gelatin, gum arabic, silicone, and so forth. Nevertheless, results emphasized the extreme difficulty of regulating the particle size to be appropriate for blood flow in the capillaries and to obtain sufficient biocompatibility. After Bangham and Horne reported in 1964 (*38*) that phospholipids assemble to form vesicles in an aqueous medium and encapsulated water-soluble materials in their inner aqueous interior (*39*), it seemed reasonable to use such vesicles for Hb encapsulation. Djordjevich and Miller in 1977 (*40*) prepared liposome-encapsulated Hb (LEH) composed of phospholipids, cholesterol, fatty acids, and so forth. The US Naval Research Laboratories and collaborators demonstrated remarkable progress in the use of LEH (*41–43*). Terumo Corp. (Tokyo) developed different LEH, so-called Neo Red Cells (*44, 45*) (Table 1).

However, some intrinsic issues of encapsulated Hbs remained, which were related mainly to the nature of molecular assembly and particle dispersion. What we call Hb-vesicles (HbV), with their high-efficiency production processes and improved properties, were established by our group based on technologies of molecular assembly in concert with precise analyses of their pharmacological and physiological aspects (*46–48*) (Tables 2 and 3). We use stable carbonylhemoglobin (HbCO) for purification with pasteurization at 60 °C for 10 h. The purity of the obtained Hb solution is extremely high (*49, 50*). Use of the stable and purified HbCO enables concentration of the Hb solution to more than 40 g/dL using ultrafiltration and easy handling of Hb encapsulation using the extrusion method,

Table 1. List of Representative Liposome-Encapsulated Hbs (LEH) Extensively Studied Aiming at Industrialization and Other Potential Encapsulated Hbs Using Biodegradable Polymers

product name	group	characteristics	current status
Hb vesicles (HbV)	Waseda Univ. and Keio Univ.	1. Pasteurization of HbCO at 60 °C for virus inactivation 2. Lipid composition to improve blood compatibility 3. PEG modification and deoxygenation for 2 yr storage 4. [Hb] = 10 g/dL	preclinical
Neo Red Cells (NRC)	Terumo Corp.	1. Inositol hexaphosphate to regulate P_{50} (= 40−50 Torr) 2. Lipids: HSPC/cholesterol/fatty acid/PEG-lipid 3. Storage in a refrigerator for 6 months 4. [Hb] = 6 g/dL	preclinical
artificial red cells (ARC)	NOF Corp. and Waseda Univ.	1. Polymerized lipids (DODPC) for stabilization 2. Storage in powdered or frozen state 3. Difficulty in degradation in RES	suspended
liposome-encapsulated Hb (LEH)	US Naval Research Laboratory	1. Freeze-dried powder with trehalose 2. Low Hb encapsulation efficiency 3. Thrombocytopenia, complement activation	suspended
synthetic erythrocytes	Rush-Presbyterian-St. Luke's Medical Center, Univ. Illinois	1. The first attempt of LEH	suspended
Hb-loaded particles (HbP)	East China Univ. of Science and Technology	1. Hb encapsulation by poly(ε-caprolactone) (PCL) and poly(ε-caprolactone-ethylene glycol) (PCL-PEG) 2. Double emulsion and solvent diffusion/evaporation method 3. Biodegradable	basic study
polymersome-encapsulated Hb (PEH)	The Ohio State Univ.	1. Self-assembly of amphiphilic diblock copolymers composed of poly(ethylene oxide) (PEO), poly(caprolactone) (PCL), and poly(lactide) (PLA) 2. Biodegradable and biocompatible	basic study

Table 2. Physicochemical Characteristics of Hb Vesicles

parameter	
particle diameter	250−280 nm
P_{50} (O_2)[a]	25−28 Torr
[Hb]	10 g/dL
[heme]	6.2 mM
[metHb]	<3%
[HbCO]	<2%
suspending medium	physiologic saline solution (0.9% NaCl)
colloid osmotic pressure	0 Torr
intracellular Hb concentration	ca. 35 g/dL
lipid composition	DPPC/cholesterol/DHSG/DSPE-PEG_{5000}
ζ potential[b]	−18.7 mV
weight ratio of Hb to lipids	1.6−1.9 (w/w)
viscosity[c]	3.8 cP
lamellarity	nearly 1
stability for storage at room temperature	>2 years, purged with N_2
circulation half-life	35 h (rats)

[a] Measured with a Hemox Analyzer (pH 7.4, 37 °C). [b] Measured with a Zeta-Sizer Nano ZS ([NaCl] = 20 mM, pH 7.4). [c] Measured with Anton Parr Rheometer M301 (268 s^{-1}, 25 °C).

Table 3. Characteristics of Hb-Vesicles As a Transfusion Alternative

1. Human derived Hb solution is purified rigorously by pasteurization and ultrafiltration. The blood type antigens and pathogens are eliminated for utmost safety.
2. Encapsulation of concentrated Hb solution (>35 g/dL), like RBCs.
3. Small particle size (250 nm) for homogeneous distribution in the plasma phase of circulating blood.
4. Shielding of the side effects of molecular Hbs by the lipid membrane.
5. PEG modification for dispersion stability for long-term storage and in the bloodstream.
6. Surface properties of HbV (PEG, negative charge, etc.) for blood compatibility.
7. Prompt degradation and excretion of the components after entrapment in RES.
8. Sufficient oxygen transporting capacity ([Hb] = 10 g/dL, *cf.* [Hb] of blood = 12−15 g/dL).
9. Physicochemical properties are easily adjustable because of the nature of the "molecular assembly".

without causing Hb denaturation. It has been confirmed that HbV encapsulates nearly 35 g/dL within a thin bilayer membrane. In final processing, CO of HbCO in HbV is photodissociated by irradiation of visible light under an O_2 atmosphere, and it converts to HbO_2 (*51*).

In fact, Hb autoxidizes to form metHb and loses its O_2-binding ability during storage and during blood circulation (*52*−*56*). For that reason, metHb formation must be prevented. A method exists to preserve deoxygenated Hbs in a liquid state from using intrinsic characteristics of Hb: the Hb oxidation rate in a solution is dependent on the O_2 partial pressure; moreover, deoxyHb is not autoxidized at ambient temperatures (*56*). In the case of HbV, not only the encapsulated Hb but also the capsular structure (liposome) must be physically stabilized to prevent irreversible intervesicular aggregation, fusion, and leakage of the encapsulated Hb.

In addition to HbV, new encapsulated Hbs without liposomes have emerged with the use of recent advanced nanotechnologies, such as polymersome (*57*) and PEG-poly(ε-caprolactone) copolymer nanoparticles (*58*). In vivo evaluation of O_2-carrying capacities of these new materials is anticipated. Encapsulation of Hb can reduce the toxicity of cell-free Hbs. However, numerous hurdles must be surmounted to realize encapsulated Hbs because of the components of the capsules themselves and their structural complexity as a molecular assembly. It is also important to consider the larger dosage requirement of encapsulated Hb for blood substitution than those of conventional drug delivery systems, which require no large dosage.

2.2. Structural Stabilization and Destabilization using Polymerization or PEG Conjugation. Liposomes, as molecular assemblies, have generally been characterized as structurally unstable. The US Naval Research Laboratory tested the addition of cryoprotectants and lyoprotectants such as trehalose to LEH for its preservation as a powder without causing hemolysis after rehydration (*59*, *60*). In addition, many researchers have developed stabilization methods for liposomes that use polymer chains (*61*−*64*). Polymerization of phospholipids that contain two dienoyl groups (1,2-dioctadecadienoyl-*sn*-glycero-3-phosphatidylcholine: DODPC) was studied extensively by our group. For example, gamma-ray irradiation induces radiolysis of water molecules and generates OH radicals that initiate intermolecular polymerization of dienoyl groups in DODPC. This method produces remarkably stable liposomes, resembling rubber balls, which are resistant to freeze−thawing, freeze−drying, and rehydration (*65*, *66*). Actually, the polymerized liposomes were so stable that they were not degraded easily in the macrophages,

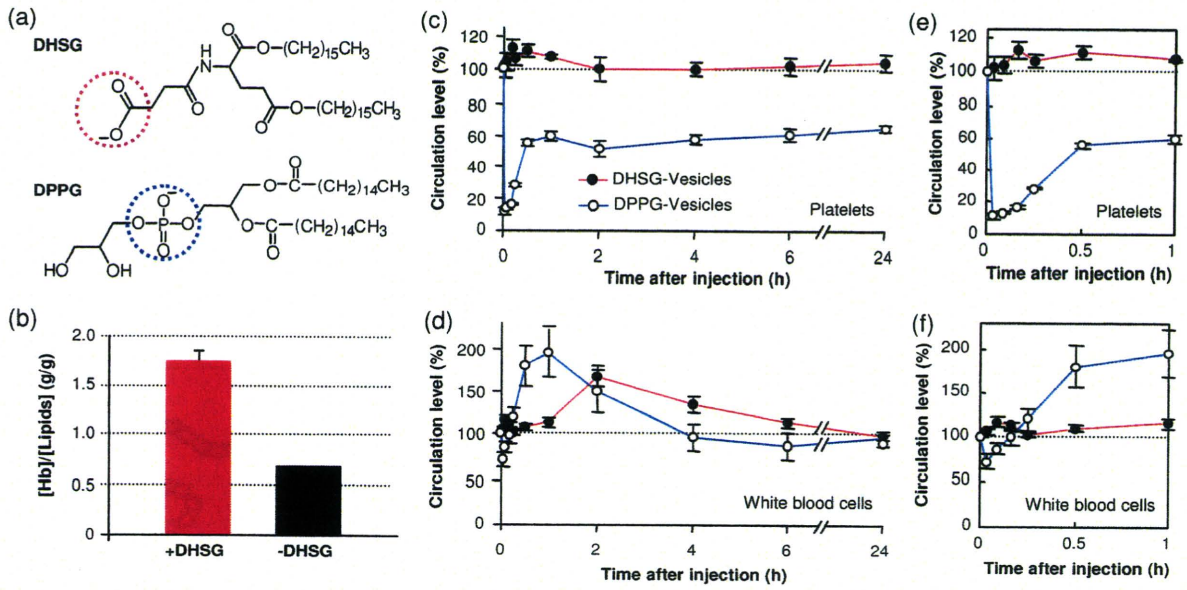

Figure 4. Effect of negatively charged vesicles on encapsulation capability and blood compatibility of HbV. (a) Chemical structures of negatively charged lipids, 1,5-*O*-dihexadecyl-*N*-succinyl-L-glutamate (DHSG) and 1,2-dipalmitoyl-*sn*-glycelo-phosphatidylglycerol (DPPG). (b) Effect of DHSG on encapsulation efficiency of Hb (35 g/dL). (c−f) Circulation levels of platelets (c) and white blood cells (d) after intravenous infusion of vesicles containing 9 mol % DHSG (DHSG-vesicles) or 9 mol % DPPG (DPPG-vesicles) in rats (lipids: 280 mg/kg body weight). The right side graphs show the initial fluctuations in platelets (e) and white blood cells (f).

even 30 days after injection (*67*). It became widely believed that polymerized lipids are inappropriate for intravenous injection because of the difficulty in excretion. Subsequently, it was clarified that selection of appropriate lipids (phospholipid/cholesterol/negatively charged lipid/PEG-conjugated phospholipid) and that their composition is important to enhance the stability of nonpolymerized liposomes (*45, 68*). Surface modification of liposomes with PEG-conjugated lipids is sufficient for dispersion stability (*69*). In fact, in comparison to RBCs, HbV is highly resistant to hypotonic shock, freeze−thawing, and enzymatic attack by phospholipase A_2 (*70*).

We investigated the possibility of long-term preservation of HbV during storage for two years through a combination of deoxygenation and PEG modification (*71*). As little as 0.3 mol % PEG-conjugated lipid stabilizes the dispersion state and prevents aggregation and fusion for two years through steric hindrance (*71−73*). The original metHb content (ca. 3%) before preservation decreased gradually to less than 1% after 1 month because of the presence of a reductant, such as homocysteine, inside the vesicles that consumed the residual O_2 and gradually reduced the trace amount of metHb. The rate of metHb formation was strongly dependent on the O_2 partial pressure: a lack of increase in the metHb formation was observed because of the intrinsic stability of the deoxygenated Hb. In fact, the metHb content did not increase for two years. These results suggest the possibility that the HbV suspension can be stored at room temperature for at least two years, which would enable stockpiling of HbV for any emergency.

2.3. Vesicular Surface Modification with PEG and Negative Charges for Blood Compatibility. Liposome is not a solute: it is a particle in a suspension. The particle surface might be recognized, leading to interaction with blood components including complements. The so-called *injection reaction*, or pseudoallergy, results from complement activation, giving rise to anaphylatoxins, which trigger various hypersensitivity reactions. This reaction is observed sometimes not only with liposomal products (*74*), but also with fat emulsions (*75*), and a perfluorocarbon emulsion (*76*). Therefore, examination of blood compatibility of encapsulated Hbs is important for clinical use. Transient thrombocytopenia and pulmonary hypertension in relation to complement activation is an extremely important hematologic effect observed in rodent models after infusion of LEH (containing DPPG: 1,2-dipalmitoyl-*sn*-glycero-3-phosphatidylglycerol) developed by the US Naval Research Laboratory (*77, 78*) and other products. In our group, exchange transfusion of prototype HbV (containing DPPG, no PEG modification) in anesthetized rats engendered transient thrombocytopenia and slight hypertension (*79*). Similar effects were also observed for administration of negatively charged liposomes (*80, 81*). The transient reduction in platelet counts caused by complement-bound liposomes was also associated with sequestration of platelets in the lung and liver. Such nonphysiological platelet activation probably engenders initiation and modulation of inflammatory responses because platelets contain several potent proinflammatory substances. A negatively charged lipid is required for encapsulating a large amount of Hb using a minimum amount of lipids (*46−48*). Therefore, we had to overcome the problem of conventional negatively charged vesicles to achieve blood compatibility. In the present formation of HbV, we use a negatively charged lipid (DHSG: 1,5-*O*-dihexadecyl-*N*-succinyl-L-glutamate) and confirmed the considerable improvement of Hb encapsulation efficiency (Figure 4a,b). It must be emphasized that the present vesicle formulation for HbV apparently does not induce thrombocytopenia or complement activation in animal experiments (Figure 4c−f) (*82, 83*), probably because the present HbV contains PEG-modification and a different type of negatively charged lipid (DHSG), not DPPG or a fatty acid.

Ikeda and his co-workers (*83−86*) thoroughly examined blood compatibility of HbV to human blood in vitro. The present PEG-modified HbV containing DHSG did not affect the extrinsic or intrinsic coagulation activities of human plasma, although HbV containing DPPG and no PEG modification tended to shorten the intrinsic coagulation time. The kallikrein-kinin cascade of the plasma was activated slightly by the prototype DPPG-HbV, but not by the present PEG-DHSG-HbV. The exposure of human platelets to high concentrations of the present HbV (up to 40%) in vitro did not cause platelet activation and did not adversely affect the formation and secretion of prothrombotic substances or proinflammatory substances that are triggered by platelet agonists. These results imply that HbV, at concentrations of up to 40%, has aberrant interactions with neither unstimulated

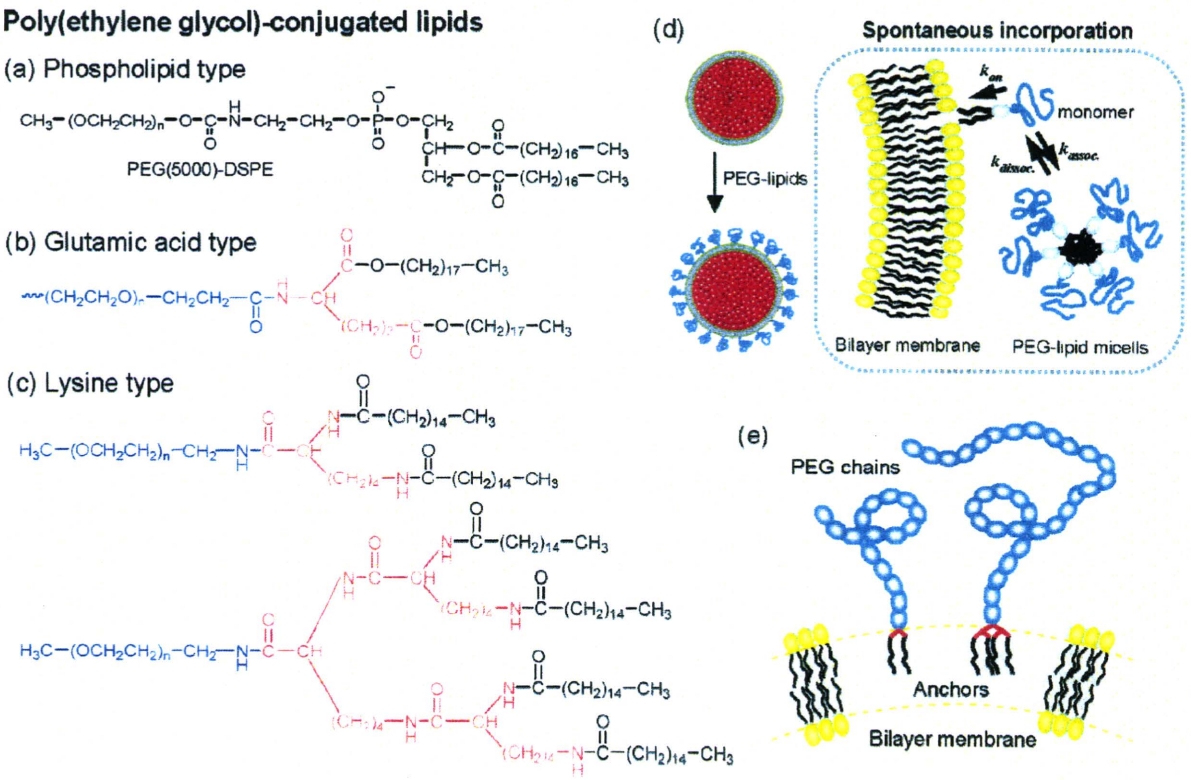

Figure 5. Surface modification of HbV with PEG chains. (a–c) Chemical structures of PEG-conjugated lipids. (a) PEG(5000)-DSPE is commercially available and widely used for surface modification of lipid vesicles. (b) Glutamic acid-type and (c) lysine-type PEG-conjugated lipids were reported previously (*87, 88*). (d) PEG-modification of the HbV using the spontaneous incorporation of a PEG-lipid into the bilayer membrane (*72*). (e) Immobilization of the large water-soluble polymers on the bilayer membranes (*87, 89*).

nor agonist-induced platelets. It can be concluded that the present PEG-DHSG-HbV has higher blood compatibility.

For surface modification of HbV with PEG chains, several PEG-conjugated lipids having amino acid backbone have been synthesized, as presented in Figure 5b,c (*87, 88*). For other applications, these PEG-conjugated lipids are available to modify the surfaces of not only HbV but also lipid vesicles. Because the PEG-lipids having a large hydrophilic group form thermodynamically unstable self-assemblies, called micelles (*73*), they easily dissociate to monomers and spontaneously incorporate only to the outer surface of preformed HbV, as illustrated in Figure 5d (*45, 72*). Using this method, the required amount of PEG-conjugated lipid can be reduced by half or less because only the outer surface of HbV requires PEG chains. In addition, the PEG chains extending from the inner surface are expected to reduce the interior volume for encapsulation because of their exclusion volume effect. Therefore, modification only to the outer surface is important to encapsulate large amounts of Hb in lipid vesicles. To immobilize the hydrophilic macromolecules stably, such as PEG chains and proteins on lipid vesicles, a large hydrophobic anchor having a tetraacyl structure has been synthesized (Figure 5c,e). It has been confirmed that this hydrophobic anchor can stably immobilize PEG chains of high molecular weight (Mw 12 500) or water-soluble proteins (*87, 89*). These surface modification technologies and lipid chemistry have been applied to the development of other functional biomaterials (*87–93*).

2.4. Circulation Time, Biodistribution, and Metabolism. The dosage of blood substitutes is expected to be considerably larger than those of other drugs, while their circulation time is considerably shorter than that of RBCs. Therefore, their biodistribution, metabolism, excretion, and side effects must be characterized in detail, especially in relation to the reticuloendothelial system (RES, alternatively, the mononuclear phagocytic system, MPS). Normally, free Hb released from RBCs is bound rapidly to haptoglobin and is consequently removed from circulation by hepatocytes. However, when the Hb concentration is greater than the haptoglobin binding capacity, unbound Hb is filtered through the kidney, where it is actively absorbed. Hemoglobinuria and eventual renal failure occur when the kidney reabsorption capacity is exceeded. The encapsulation of Hb in vesicles completely suppresses renal excretion. However, HbV in the bloodstream is ultimately captured by phagocytes in the RES in much the same manner as senescent RBCs are, as confirmed by radioisotope ^{99m}Tc-labeled HbV injection (*42, 94*). The circulation half-life is dose-dependent: for the dosage of 14 mL/kg body weight, the circulation half-life was 34.8 h in rats and 62.6 h in rabbits (Figure 6a). The HbV are finally distributed mainly in the liver, spleen, and bone marrow (Figure 6b). The species-dependent circulation time is inferred to be dependent upon the species-specific weight balance of phagocyte organs, particularly the liver, spleen, and bone marrow, against body weight (*94*). The circulation half-life in the case of the human body can be estimated as about 2–3 days at the same dosage.

It is generally accepted that the liposome clearance by RES at a small dosage is accelerated by opsonization (absorption of plasma proteins such as antibodies and complements on the liposomal surface). In fact, PEG-modification prevents opsonization for prolonged circulation times (*95*). However, considering a condition in which the dosage of HbV is extremely high and requires a considerable amount of opsonins, and in which HbV does not induce complementary activation (*82, 83*), then opsonin-dependent phagocytosis would not be a major component in the case of HbV with a large dosage. Actually, opsonin-independent phagocytosis, a direct recognition by macrophages, has been clarified in some studies (*96, 97*).

Analysis of the spleen by transmission electron microscopy (TEM) 1 day after infusion of HbV revealed the presence of HbV particles in the phagosomes of macrophages (*98*) (Figure

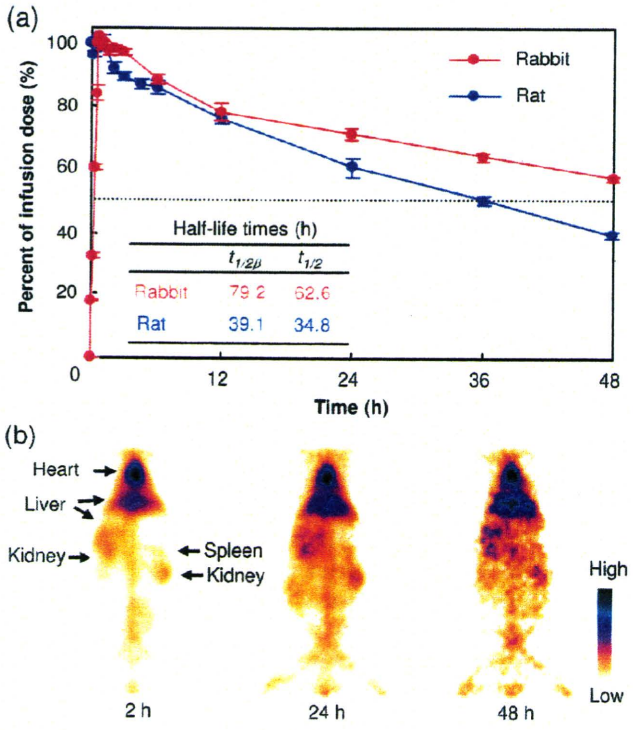

Figure 6. Circulation kinetics and organ distribution of HbV labeled with technetium-99m after top-loading intravenous infusion (14 mL/kg) in rats and rabbits (*94*). (a) Elimination profiles of HbV from blood. (b) Static gamma camera images of a rabbit acquired at 2, 24, and 48 h after HbV infusion.

7). However, after 7 days, the HbV structure cannot be observed. We confirmed transient splenomegaly with no irreversible damage to the organs and complete metabolism within a week. The phagocytic activity transiently, but not completely, decreased 1 day after injection, and it turned to increasing at 3 days. The influence on the defense function and its mechanism has been carefully examined in the ongoing research. Immunochemical staining with a polyclonal anti-human Hb antibody was used as the marker of Hb in the HbV. Results clarified that HbV had almost disappeared in both the spleen and liver after 7 days.

Bilirubin and iron are believed to be released during metabolism of Hb, but our animal experiments of topload infusion, daily repeated infusions, and 40% blood exchange showed that neither of those products increased in the plasma within 14 days (*99*−*101*). Bilirubin would normally be excreted in the bile as a normal pathway; no obstruction or stasis of the bile is expected to occur in the biliary tree. Berlin blue staining revealed considerable deposition of hemosiderin in the liver and spleen, even after 14 days. Moderate splenomegaly and hemosiderin deposition were also confirmed in the spleen after injection of stored RBCs, partly because of the accumulation and degradation of stored RBCs with lowered membrane deformability and shortened circulation half-life (*101*).

As for membrane components of Hb-vesicles, the plasma cholesterol level elevated transiently 3 days after injection: cholesterol was released from macrophages after degradation of HbV in phagosomes (*99, 101*). It was recently clarified using ^{3}H-cholesterol that cholesterol of HbV is released from macrophages to blood; it is ultimately excreted in feces. The PEG chain is widely used for surface modification of liposomal products. The chemical cross-linker succinic acid ester of PEG-conjugated phospholipid is susceptible to hydrolysis to release PEG chains during metabolism. Actually, immunohistochemistry using an anti-methoxy-PEG antibody clarified that PEG had disappeared from the liver and spleen in one week (*102*). The

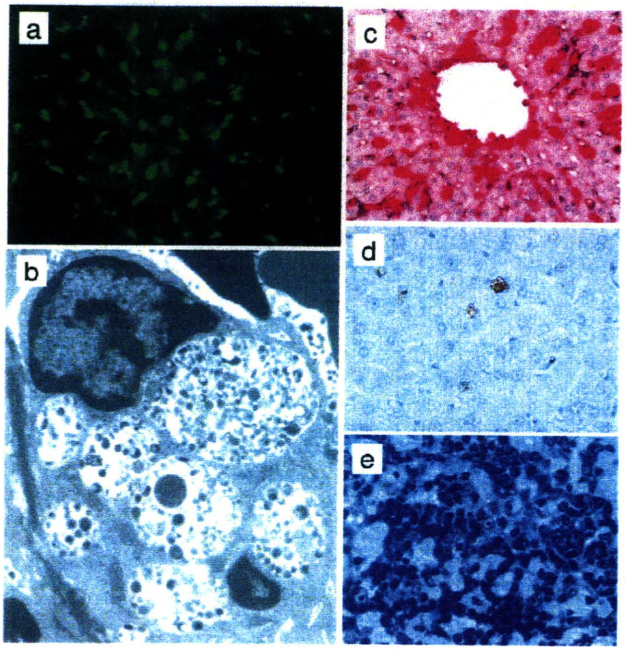

Figure 7. Histopathological examination of livers and spleens of rodents after injection of HbV. (a) Hamster liver 1 h after injection of fluorescence-labeled HbV, observed by a confocal laser scanning microscopy. The strong fluorescence indicates that HbV particles accumulate in Kupffer cells. (b) TEM of rat spleen macrophage 1 day after injection of HbV. The small black dots are HbV particles in phagosomes. The particles disappeared within a week (data not shown) (*98*). (c) Rat liver 1 day after injection of HbV. It was immunohistochemically stained with anti-human Hb antibody. The red parts indicate the presence of human Hb in HbV. It disappeared within a week (data not shown) (*98*). (d) Rat liver 7 day after injection of HbV. It was immunochemically stained with anti-methoxy-PEG antibody. The brown parts indicate the presence of PEG derived from PEG-lipid of HbV during the degradation. Fourteen days after injection, PEG was not detectable (data not shown) (*102*). (e) Rat spleen 3 days after 40% exchange transfusion with HbV. It was stained with Giemsa method. A large amount of blue cells, erythroblasts, are seen, indicating the enhanced hematopoiesis for the complete recovery of hematocrit within one week, while HbV are degraded in RES (*101*).

released PEG chains, which are known as inert macromolecules, are expected to be excreted in urine through the kidneys (*103*).

To determine the physiological capacity of RES for degradation of HbV, we tested massive intravenous doses by daily repeated infusion of 10 mL/kg body weight/day into Wistar rats for 14 days. The cumulative dosage was 140 mL/kg body weight (Hb and lipids, 20 689 mg/kg body weight). The total volume was equal to 2.5 times the total blood volume (56 mL/kg body weight) (*100*). Although splenohepatomegaly was considerable, all rats tolerated the infusions; their body weight increased during the succeeding 14 days until their intended sacrifice. The phagocyted HbV had disappeared, though the considerable hemosiderin deposition was confirmed in the spleen, liver, kidney, adrenal grand, and bone marrow. We were unable to define a lethal dose of HbV in this experiment.

The profile of liposome clearance is species-dependent. More precise data are necessary to extrapolate the phenomena observed in animal experiments to humans. However, these results imply that the metabolism of HbV and excretion are within the physiological capacity that has been well-characterized for the metabolism of senescent RBCs and conventional liposomal products.

2.5. Regulation of O_2 Transporting Capability (MetHb Reduction, $P_{50}(O_2)$). Actually, Hb encapsulation provides a unique opportunity to add new functions to particles by coencapsulation or embedding of functional molecules (*52*−*56, 104*−*106*). MetHb formation of HbV during the

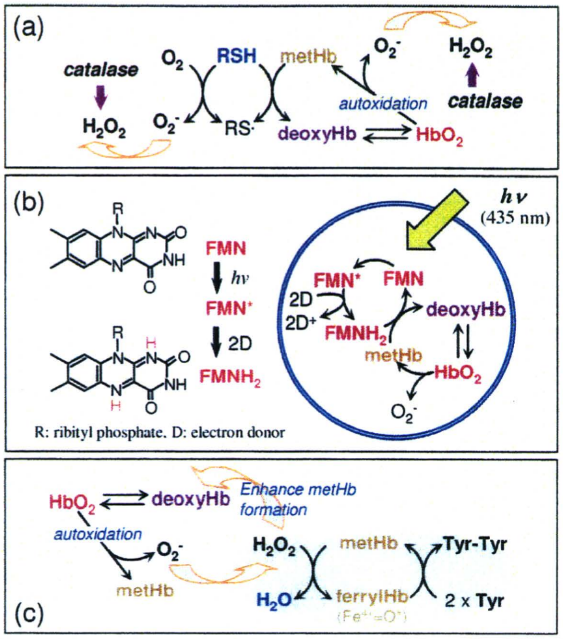

Figure 8. Artificial metHb reduction systems in HbV. (a) Coencapsulation of thiols (RSH), such as glutathione and homocyteine, reduces metHb. However, thiols react with O_2 to generate O_2^- and H_2O_2. A more reactive thiol such as cysteine shows extremely rapid reaction with O_2 and adversely facilitates metHb formation. Coencapsulation of catalase effectively eliminates H_2O_2 and prevent such reactions (*52, 53, 56*). (b) Photoreduction system by coencapsulation of flavin monomucleotide (FMN) and an electron donor such as EDTA and methionine. Visible light irradiation (435 nm) primarily converts FMN to the photoexcited triplet FMN*, and this reacts with two electron donors (D) to generate $FMNH_2$. MetHb is rapidly reduced once $FMNH_2$ is produced (*54*). (c) During autoxidation of Hb and in blood circulation, H_2O_2 is a potent metHb enhancer. A combination of L-tyrosine (Tyr) and metHb effectively eliminates H_2O_2 and prolongs the functional lifetime of HbV (*55*).

preservation is completely prevented simply by deoxygenation. However, autoxidation of HbO_2 is initiated once HbV is administered into the bloodstream because the entire metHb enzymatic system is eliminated during the Hb purification for the utmost safety from infection. An artificial metHb reducing system is required to prolong the O_2-carrying capacity of HbV. We have tested coencapsulation of reductants to directly reduce metHb and a photoreduction system using a photosensitizer such as flavin mononucleotide (FMN). A more practical method is to create an artificial enzymatic system using L-tyrosine (Tyr) and metHb that eliminates H_2O_2 as does catalase (Figure 8).

Without a chemical modification of Hb, O_2 binding affinity (expressed as $P_{50}(O_2)$, O_2 tension at which Hb is half-saturated with O_2) of HbV can be regulated by coencapsulation of an allosteric effector (*105, 106*) (Figure 9a). The $P_{50}(O_2)$ of purified Hb in a saline solution (in the presence of Cl^-) is about 14 Torr; Hb strongly binds O_2 and does not release O_2 at 40 Torr (partial pressure of mixed venous blood). Historically, it has been regarded that the O_2 affinity is expected to be regulated similarly to that of RBC, namely, about 25−30 Torr, using an allosteric effector or by a direct chemical modification of the Hb molecules. This enables sufficient O_2 unloading during blood microcirculation, as evaluated by the arterio-venous difference in the levels of O_2 saturation in accordance with an O_2 equilibrium curve. Pyridoxal 5′-phosphate (PLP) is coencapsulated in HbV as an allosteric effector to regulate $P_{50}(O_2)$ (*105, 106*). The main binding site of PLP is the N-terminal of the α-chain and β-chain and β-82 Lysine within the β-cleft, which is part of the binding site of the natural allosteric effector, 2,3-diphosphoglyceric acid (2,3-DPG). The bound PLP retards the dissociation of the ionic linkage between the β-chains of Hb during conversion of deoxy to oxyHb in the same manner as 2,3-DPG does. Therefore, the O_2 affinity of Hb decreases in the presence of PLP. The $P_{50}(O_2)$ of HbV can be regulated to 8−150 Torr by coencapsulating the appropriate amount of PLP or inositol hexaphosphate as an allosteric effector. Equimolar PLP to Hb (PLP/Hb = 1/1 by mol) was coencapsulated, and $P_{50}(O_2)$ was regulated to 18 Torr. Furthermore, $P_{50}(O_2)$ was regulated to 32 Torr when the molar ratio PLP/Hb was 3/1. The O_2 affinities of HbV can be regulated easily without changing other physical parameters, whereas in the case of the other modified Hb solutions, their chemical structures determine their O_2 binding affinities. Consequently, regulation is difficult. The present HbV contains PLP at PLP/Hb = 2.5 by mol; the resulting $P_{50}(O_2)$ is about 25−28 Torr, which shows sufficient O_2 transporting capacity as a transfusion alternative. Actually, HbV has been shown to provide O_2-transport capacity that is both sufficient and comparable to that of RBCs in experiments related to extreme blood exchange (*68, 69, 79, 105, 107, 108*) and fluid resuscitation from hemorrhagic shock (*102, 109−112*) (Figure 10). A recent experiment of HbV as a priming solution for cardiopulmonary bypass (CPB) in a rat model showed that HbV protects neurocognitive function by transporting O_2 to brain tissue even when the hematocrit is reduced markedly (*113*).

The appropriate O_2 binding affinities for O_2 carriers have not yet been decided completely. However, the easy regulation of the O_2 binding affinity might be useful to meet the requirement of clinical indications such as oxygenation of ischemic tissues. The $P_{50}(O_2)$ of HbV without PLP and Cl^- is 8−9 Torr. This formulation is effective for targeted O_2 delivery to anoxic tissues caused by reduced blood flow (*107, 114, 115*).

2.6. Rheological Properties and Their Physiological Implications for Tissue Oxygenation. The extremely high concentration of the HbV suspension ([Hb] = 10 g/dL; [lipids] = 6 g/dL, volume fraction, ca. 40 vol %) imparts an O_2 carrying capacity that is comparable to that of blood. The HbV suspension does not possess a colloid osmotic pressure (COP), because one HbV particle (ca. 250 nm diameter) contains about 30 000 Hb molecules. In fact, HbV acts as a particle, not as a solute. Therefore, HbV must be suspended in or coinjected with an aqueous solution of a plasma substitutes. This requirement is identical to that for emulsified perfluorocarbon, which does not possess COP (*116, 117*); it contrasts to characteristics of other Hb-based O_2 carriers, intramolecular cross-linked Hbs, polymerized Hbs, and polymer-conjugated Hbs, which all possess very high COP as protein solutions (*15, 118*) (Figure 9b).

Animal tests of HbV suspended in plasma-derived HSA or rHSA showed an O_2 transporting capacity that is comparable to that of blood (*110, 113*). We reported previously that HbV suspended in plasma-derived HSA or rHSA was almost Newtonian: no aggregation was detected microscopically (*68, 69*). In Japan, rHSA was very recently approved for clinical use, in May 2008 (*119*), but various plasma substitutes are used worldwide, such as hydroxylethyl starch (HES), dextran (DEX), and modified fluid gelatin (MFG). The selection among these plasma substitutes is best determined not only according to their safety and efficacy, but also according to their associated price, experience of clinicians, and customs of respective countries. Water-soluble polymers generally interact with particles such as polystyrene beads, liposomes, and RBCs to induce aggregation or flocculation (*120, 121*). For that reason, it is important to determine the compatibility of HbV with these plasma substitutes. With that background, we studied rheological properties of HbV suspended in these plasma substitute solutions using a complex rheometer and a microchannel array (*122*). The rheological property of an Hb-based O_2 carrier is important

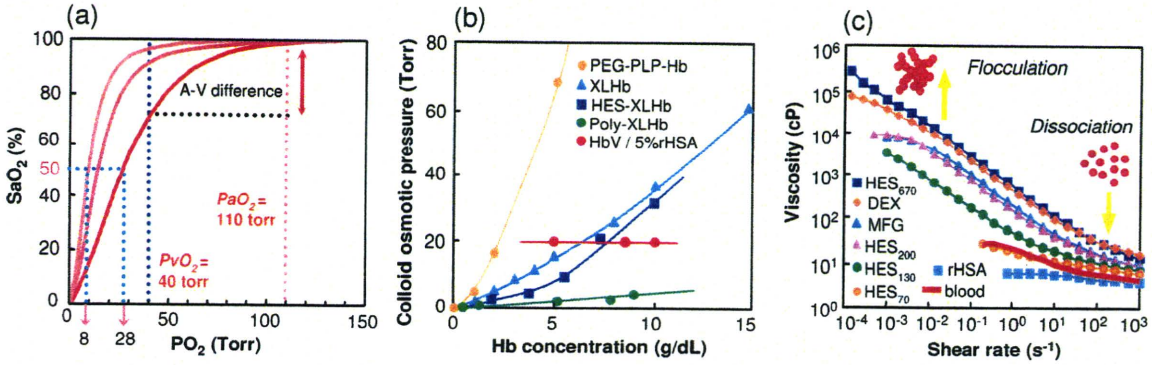

Figure 9. Regulation of physicochemical properties of HbV for versatile applications. (a) Oxygen dissociation curves of HbVs. Oxygen affinity (P_{50}, partial pressure of oxygen at which Hb is half-saturated with oxygen) is regulated by coencapsulation of PLP (*105, 106*). (b) Colloid osmotic pressure (COP) of chemically modified Hb solutions increase with the Hb concentration (*15*). In contrast, HbV particles have no oncotic effect. The figure shows 20 Torr when HbV is suspended in 5% rHSA. XLHb, intramolecularly cross-linked Hb. (c) Rheological properties of HbV suspended in various plasma substitute solutions (*122*). [Hb] = 10 g/dL, 25 °C.

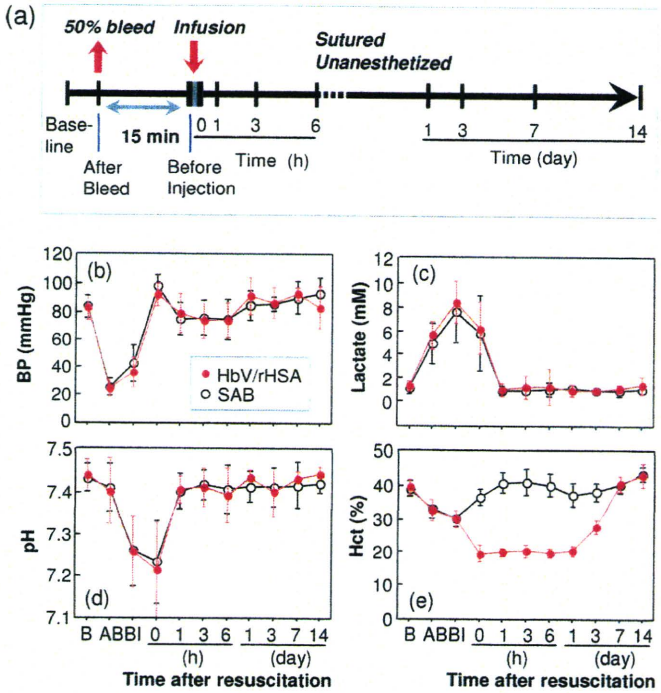

Figure 10. (a) Scheme depicting the experimental protocol of hemorrhagic shock and resuscitation (*102*). Shock was induced by withdrawing 50% of circulating blood volume from Wistar rats. After 15 min, they were resuscitated with either HbV suspended in recombinant human serum albumin (HbV/rHSA) or shed autologous blood (SAB). (b) blood pressure, (c) lactate, (d) pH, and (e) hematocrit (Hct). Mean ± SD. B, Baseline; AB, after bleeding; BI, before injection (B-6 h, n = 24; 1−14 days, n = 5).

because the infusion amount is expected to be considerably large, which might affect the blood viscosity and hemodynamics.

The HbV suspended in rHSA was nearly Newtonian (Figure 9c). Its viscosity was similar to that of blood, and the mixtures with RBCs at various mixing ratios showed viscosities of 3−4 cP. Other polymers, HES, DEX, and MFG, induced flocculation of HbV, possibly by depletion interaction, and rendered the suspensions as non-Newtonian with the *shear-thinning* profile (*122*). These HbV suspensions showed high viscosity and a high storage modulus (G') because of the presence of flocculated HbV. On the other hand, HbV suspended in rHSA exhibited a very low G'. The viscosities of HbV suspended in DEX, MFG, and high-molecular-weight HES solutions responded quickly to rapid step changes of shear rates of 0.1−100 s^{-1} and a return to 0.1 s^{-1}, indicating that flocculation formation is both rapid and reversible. Microscopically, the flow pattern of the flocculated HbV perfused through microchannels (4.5 μm deep, 7 μm wide, 20 cmH_2O applied pressure) showed no plugging. Furthermore, the time required for passage was directly related to the viscosity.

Table 4. Publications of Preclinical Studies Aiming at Applications of Hb-Vesicles for a Transfusion Alternative and for Oxygen Therapeutics

indication	ref
1. Resuscitative fluid for hemorrhagic shock	102, 109−112
2. Hemodilution	68, 69, 79, 101, 105, 107, 108
3. Priming fluid for extracorporeal membrane oxygenator (ECMO) for cardiopulmonary bypass	113
4. Perfusate for resected organs (transplantation)	24, 129
5. Oxygenation of ischemic brain (stroke)	130
6. Oxygenation of ischemic skin flap (plastic surgery)	115, 127, 128
7. Tumor oxygenation for sensitization to irradiation	131
8. CO carrier for cytoprotection at reperfusion	132

It has been regarded that lower blood viscosity after hemodilution is effective for tissue perfusion. However, microcirculatory observation shows that, in some cases, lower "plasma viscosity" decreases shear stress on the vascular wall, causing vasoconstriction and reducing the functional capillary density (*123*). Therefore, an appropriate viscosity might exist, which maintains the normal tissue perfusion level. The large molecular dimension of HbV can result in a transfusion fluid with high viscosity. A large molecular dimension is also effective to reduce vascular permeability and to minimize the reaction with NO and CO as vasorelaxation factors (*24, 25, 30, 31*) (see Figure 3). These new concepts suggest reconsideration of the design of artificial O_2 carriers (*124*). Actually, new products are appearing, although they are in the preclinical stage, not only HbV but also zero-link polymerized Hb (*125*) and others with larger molecular dimensions and higher O_2 affinities (*126*). Erni et al. clarified that HbV with a high O_2 binding affinity (low $P_{50}(O_2)$, such as 8−15 Torr) and high viscosity (such as 11 cP) suspended in a high-molecular-weight HES solution was effective for oxygenation of an ischemic skin flap (*115, 127, 128*). That study showed that HbV retains O_2 in the upper arterioles, then perfuses through collateral arteries and delivers O_2 to the targeted ischemic tissues, a concept of targeted O_2 delivery by an Hb-based O_2 carrier (*114*). A high O_2 binding affinity (low $P_{50}(O_2)$) would also be effective to improve the O_2 saturation of Hb in pulmonary capillaries when exposed to a hypoxic atmo-

Figure 11. Crystal structure of HSA with myristate (PDB ID: 1BJ5) from ref (*136*).

sphere or with an impaired lung function. Some plasma substitutes cause flocculation of HbV and hyperviscosity. However, reports show that hyperviscosity would not necessarily be deteriorative and might be, in some cases, advantageous in the body (*32*). HbV provides a unique opportunity to manipulate the suspension rheology, $P_{50}(O_2)$, and other physicochemical properties, not only as a transfusion alternative, but also for other clinical applications such as oxygenation of ischemic tissues and ex vivo perfusion systems (*129*−*132*) (Table 4).

3. ALBUMIN-HEMES AS O_2 CARRYING PLASMA PROTEINS

3.1. HSA Incorporating Synthetic Fe^{2+} Porphyrin (HSA-FeP). HSA (Mw: 66 500) has a remarkable ability to bind a wide variety of exogenous compounds in the human circulatory system (*133*). This carrier protein comprises 3 homologue helical domains (I−III) with 9 loops formed by 17 disulfide linkages; each domain contains 2 subdomains (A and B) (Figure 11) (*134*−*137*). It is known that many common drugs such as warfarin, diazepam, and ibuprofen bind to one of the two primary sites (site 1 in subdomain IIA, site 2 in subdomain IIIA) (*138*). In fact, HSA helps to solubilize these compounds to achieve high concentration in the bloodstream; otherwise, they would easily aggregate and be poorly distributed.

In 1995, we found that tetrakis(*o*-pivalamido)phenylporphinatoiron bearing a covalently linked proximal imidazole (FeP**1**, Figure 12) was incorporated into HSA, yielding a red HSA-FeP**1** hybrid (*11*). This synthetic hemoprotein can reversibly bind and release O_2 under physiological conditions (pH 7.4, 37 °C) in much the same way as Hb. The HSA host adsorbs a maximal eight FeP**1** molecules. Their stepwise binding constants (K_1−K_8) range from 1.2×10^6 to 1.2×10^4 (M^{-1}) (Table 3) (*139*, *140*). Solution properties of the HSA-FeP**1** solution ([rHSA] = 5 wt %, FeP/HSA=1−8, mol/mol) are almost identical to those of HSA itself: the specific gravity, 1.013; viscosity, 1.1 cP; and COP, 20 Torr. Circular dichroism (CD) spectroscopy and isoelectric focusing measurement revealed that the second-order structure and surface charge distribution of HSA were unaltered after binding of FeP**1**. The obtained solution showed a long shelf-life of over two years at room temperature (*141*). Furthermore, HSA-FeP**1** has no effect on the morphology of blood cell components (*142*) and does not engender immunological reaction and platelet activation (*143*). Upon addition of O_2 gas through this solution, the visible absorption spectrum immediately changed to that of the O_2 adduct complex. After exposure to CO gas, a stable carbonyl complex of HSA-FeP**1** was formed (*139*, *140*). The coordination structure of FeP**1** and spin-state of the central ferrous ion was characterized by IR, resonance Raman, and magnetic circular dichroism (MCD) spectroscopy (*139*, *140*, *144*). The carbonyl HSA-FeP**1** moved to the NO adduct complex after bubbling NO gas (*145*). Subsequent ESR spectroscopy revealed that FeP**1** in albumin formed a six-coordinate nitrosyl complex. The proximal imidazole moiety does not dissociate from the central ferrous ion when NO binds to the trans side (*146*).

The $P_{50}(O_2)$ value of HSA-FeP**1** is always constant (33 Torr, 37 °C) independent of the binding number of FeP**1** (eq 1, Table 5)

$$\text{HSA-FeP} + \text{L} \underset{k_{off}(\text{L})}{\overset{k_{on}(\text{L})}{\rightleftarrows}} \text{HSA-FeP(L)} \quad [\text{L}: O_2 \text{ or CO}]$$

$$K(\text{L}) = [P_{50}(\text{L})]^{-1} = k_{on}(\text{L})/k_{off}(\text{L}) \quad (1)$$

The O_2 binding equilibrium curve shows no cooperativity. However, the O_2 transporting efficiency between the lungs [$P(O_2)$: ca. 110 Torr] and muscle tissue [$P(O_2)$: ca. 40 Torr] is 22%, which is identical to that for RBC.

The O_2 association and dissociation rate constants [$k_{on}(O_2)$ and $k_{off}(O_2)$] can be measured using laser flash photolysis (*147*, *148*). Interestingly, the rebinding process of O_2 to HSA-FeP**1** included two phases (fast and slow phase), perhaps because of the different environment around each FeP**1** in the protein (*149*). The $P_{50}(O_2)$ value can be controlled by tuning the chemical structure of FeP**1**. We have synthesized quantities of Fe(II)porphyrins (Figure 12) and evaluated the O_2 binding parameters of their HSA-FeP hybrids (Table 6).

Actually, FeP**2** has a bulky 1-methylcyclohexanamide group on the porphyrin ring plane (*150*). The O_2 binding affinity of HSA-FeP**2** [$P_{50}(O_2)$: 35 Torr] was almost identical to that of HSA-FeP**1**. However, the stability of the oxygenated complex increased to 4.5 times its usual value [half-life $\tau_{1/2}(O_2)$, 9 h; pH 7.3; 37 °C] (*150*).

In general, the basicity and structure of the proximal base greatly influences the O_2 binding property of Fe^{2+}porphyrin. Both FeP**3** and FeP**4**, similar analogues having an His ligand, showed high O_2 binding affinities [$P_{50}(O_2)$: 3 Torr] (Figure 13, Table 6). Kinetically, substitution of the 2-methylimidazole to His reduces the O_2 dissociation rate constant (*150*). Although one might think that high O_2 binding affinity is not useful as a blood substitute, it can be efficient for oxygenation of hypoxic regions in tumors. Furthermore, the HSA-FeP**4** showed long $\tau_{1/2}(O_2)$ of 25 h (37 °C), which is 13-fold longer than that of HSA-FeP**1**.

Another HSA-FeP**5**, in which the active porphyrin has 3-methyl-L-hisitidine as a proximal base, exhibits an extraordinarily high O_2 binding affinity [$P_{50}(O_2)$: 1 Torr] that approaches those of relaxed-state Hb and Mb (*151*). It is remarkable that replacement of the 3-methyl-L-histidine moiety by 1-methyl-L-histidine isomer (HSA-FeP**6**) reduced O_2 binding affinity to 1/35th of its former level. The low O_2 affinity of FeP**6** is predominantly reflected by the high $k_{off}(O_2)$ value. The axial Fe−N(1-methyl-L-histidine) coordination might be restrained by steric interaction between the 4-methylene group of the His ring and the porphyrin plane (*151*).

The proximal histidyl side chain can be introduced easily into the β-pyrrolic position of the porphyrin via an acyl bond in two steps, FeP**7** (*152*). Although an electron-withdrawing acyl group is bound at the porphyrin periphery, the O_2 binding affinity of HSA-FeP**7** is slightly higher than that of HSA-FeP**4**. The rigid His-Gly(carboxy)butanoyl spacer of FeP**7** probably produces a favorable geometry to fix the imidazole onto the central Fe^{2+} of the porphyrin.

Double-sided porphyrins (FeP**8**, FeP**9**, and FeP**10**) were also incorporated into HSA (*153*). We expected that steric encumbrances on both sides of the porphyrin enable the HSA-FePs to form a stable O_2 adduct complex. Actually, the $\tau_{1/2}(O_2)$ of HSA-

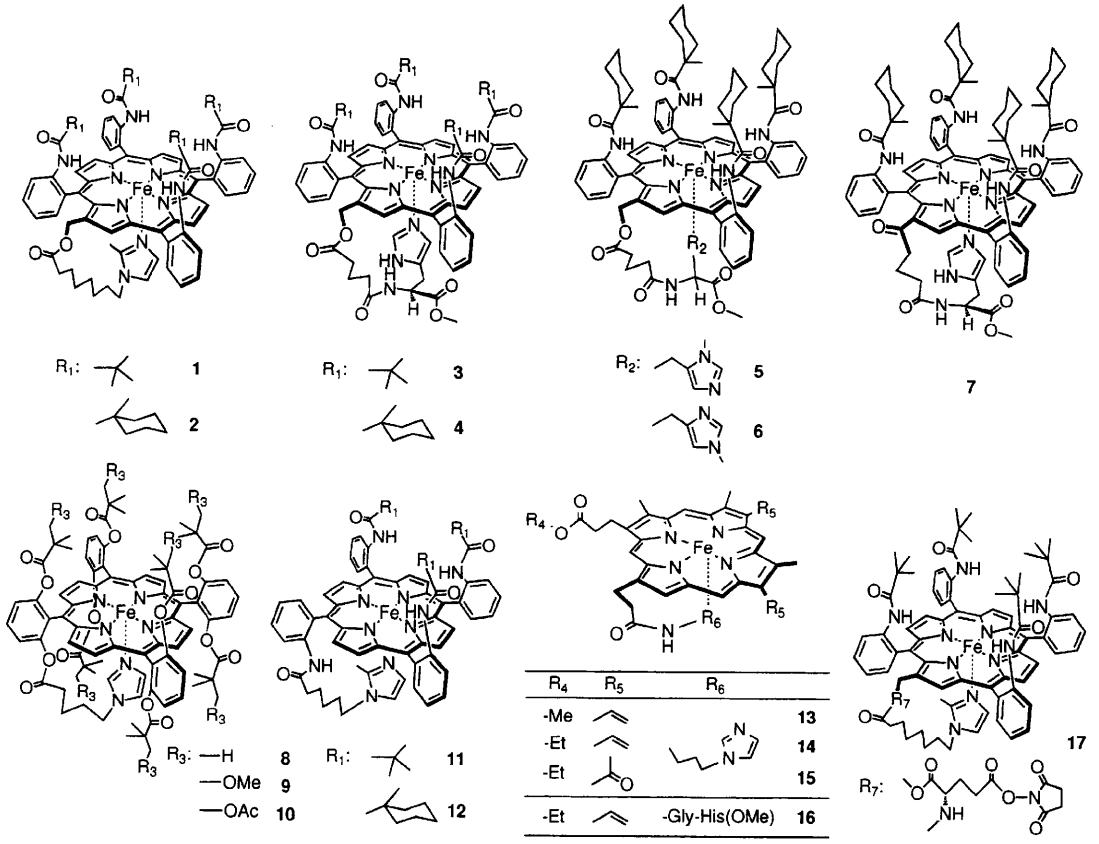

Figure 12. Structure of FePs in HSA-FePs.

Table 5. Solution Properties and Characteristics of HSA-FeP1

binding number of FeP1 (n)	1−8
binding constant of FeP1	$1.2 \times 10^6 - 1.2 \times 10^4$ M^{-1}
M_w	$(66.5 + 1.3n)$ kDa
pI	4.8
viscosity[a,b]	1.1 cP
COP[a,b,c]	20 Torr
shelf life[a,d]	>2 years

[a] In phosphate buffered solution (pH 7.3), [HSA]: 5 g/dL. [b] At 37 °C. [c] A membrane filter with a cutoff (M_w, 30×10^3) was used. [d] At 25 °C.

FeP**8** was 5 h, which is 2.5-fold longer than that of HSA-FeP**1**. In addition, HSA-FeP**8** showed high stability against hydrogen peroxide. The HSA incorporating double-sided porphyrins would be useful for the synthetic analogue of the oxidation enzyme.

Tailed porphyrins having an α,α,α,β-conformer, FeP**11** and FeP**12**, were synthesized easily via four steps from atropisomers of tetrakis(*o*-aminophenyl)porphyrin relative to eight steps of FeP**1** (*154*). Although HSA-FeP**12** binds O_2 reversibly, HSA-FeP**11** was quickly oxidized by O_2. We concluded that the 1-methylcyclohexanamide groups are necessary for the tailed porphyrin to form an O_2 adduct complex under physiological conditions.

Investigations have also revealed that heme [Fe^{2+} protoporphyrin IX; protoheme] derivatives having a proximal base at the propionate side chain (FeP**13**−FeP**16**) were incorporated into HSA (*155, 156*). The oxidation process of HSA-FeP**13**(O_2) to the inactive ferric state obeyed first-order kinetics, suggesting that the μ-oxo dimer formation was prevented by the immobilization of FeP**13** into albumin. In fact, HSA-FeP**15** showed lower O_2 binding affinity [high $P_{50}(O_2)$] than the others did. The acetyl groups at the 3,8-positions of FeP**15** decrease the electron density of the porphyrin macrocycle, thereby reducing the O_2 binding affinity. Actually, HSA-FeP**16**, in which the His-Gly tail coordinates to the Fe^{2+} center, showed the most stable O_2 adduct complexes [$\tau_{1/2}(O_2)$, 90 min; pH 7.3; 25 °C] of any of these heme compounds.

3.2. Surface-Modified HSA-FeP with PEG. A remaining defect of HSA-FeP is that the active Fe^{2+} porphyrin sites dissociate slowly from HSA when infused into animals because FeP is bound noncovalently to albumin. One possible solution is to bind the FeP molecule covalently to the protein. We have synthesized FeP**17** having a succinimide side chain; it can react with the Lys amino group of HSA (*157*). The O_2 binding property of HSA-FeP**17** is almost identical to that of HSA-FeP**1**.

Another approach is surface modification with PEG. Actually, PEG decollations of proteins and liposomes are well-known to enhance their plasma half-life, thermostability, nonimmunogenicity, and solubility in organic solvents (*158−163*). We surmised that surface modification of HSA-FeP**2** by PEG might help to prolong the circulation lifetime of FeP**2** and retain its O_2 transporting ability in vivo for a long period. Consequently, HSA-FeP**2** (FeP**2**/HSA = 4/1, mol/mol) was modified with maleimide-PEG, and the solution properties, O_2 binding behavior, and circulatory persistence of the PEG-modified HSA-FeP**2** [PEG(HSA-FeP**2**)] were examined (*164*). A thiolation reagent, iminothiolane, first reacted with the Lys amino groups of HSA to create active thiols that bind to α-maleimide-ω-methoxy PEG (Figure 14a). Mass spectroscopy measurements and quantification of the mercapro group of PEG(HSA-FeP**2**) revealed the conjugation of six PEG chains on the HSA-FeP**2** surface. The initial FeP**2**/HSA ratio 4/1 (mol/mol) was unchanged after the PEG binding. The adjustment of viscosity is important to design an artificial O_2 carrier. Maintenance of viscosity is necessary to preserve shear stress on the vascular wall that prevents loss of the functional capillary density (*123, 165*). The viscosity and COP of PEG(HSA-FeP**2**) were modulated to some degree by changing the molecular weight of PEG [M_w: 2×10^3 (PEG_{M2}) and 5×10^3 (PEG_{M5})] (Figure 14b). In fact, PEG_{M2}(HSA-FeP**2**) showed almost identical values of viscosity

Table 6. O_2 Binding Properties of HSA-FePs in Phosphate Buffered Solution (pH 7.3, 25 °C)

	$k_{on}(O_2)$ (μM^{-1} s^{-1})		$k_{off}(O_2)$ (ms^{-1})			
FeP	fast	slow	fast	slow	$P_{50}(O_2)^a$ (Torr)	refs
1	34	9.5	0.75	0.20	13 (33)	139, 149, 150
2	46	7.3	0.98	0.16	13 (35)	150
3	36	6.1	0.059	0.010	1 (3)	150
4	54	8.8	0.089	0.014	1 (3)	150
5	54	6.8	0.02	0.0024	0.2 (1)	151
6	54	8.1	0.62	0.093	7 (22)	151
7	34	4.5	0.045	0.0059	0.8 (2)	152
8	11	1.5	0.50	0.069	28	153
9	11	2.0	0.41	0.076	23	153
10	8.9	2.3	0.34	0.088	23	153
12	29	4.4	1.10	0.16	22 (45)	154
13	–	–	–	–	0.1	155, 156
14	–	–	–	–	0.1	155, 156
15	–	–	–	–	0.4	156
16	–	–	–	–	0.1	155, 156
17	28	–	0.33	–	9 (27)	157

[a] At 37 °C in parentheses.

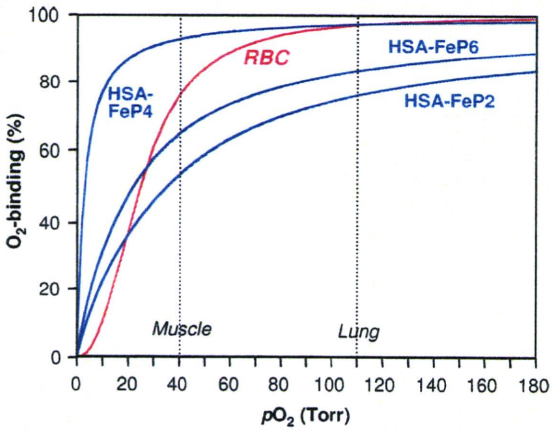

Figure 13. O_2 binding equilibrium curve of HSA-FePs under physiological conditions (pH 7.3, 37 °C).

and COP to those of the nonmodified HSA-FeP2. In contrast, PEG_{M5}(HSA-FeP2) showed a higher viscosity and more pronounced hyperoncotic property relative to those of HSA-FeP2. Nevertheless, PEG_{M5} conjugate may be useful as an efficient plasma expander (*118*, *166*).

Under physiological conditions, PEG_{Mn}(HSA-FeP2) binds and releases O_2. The $P_{50}(O_2)$ values were almost identical to those of the original HSA-FeP2, indicating that the O_2 binding equilibrium was not influenced by the presence of the PEG chains (Figure 14b). Surface modification by PEG delays proton-driven oxidation of the O_2 adduct complex, giving HSA-FeP2 the $\tau_{1/2}(O_2)$ of 12 h, which is almost equal to that of a natural hemoprotein, Mb [$\tau_{1/2}(O_2)$, 12 h; pH 7, 35 °C] (*167*). The conjugated PEG might change the local proton concentration of the HSA interior compared to the outer aqueous solution.

The circulation persistence of FeP2 in the bloodstream was measured after administration of PEG_{Mn}(HSA-FeP2) to anesthetized rats (*164*). The PEG_{Mn}(HSA-FeP2) solution (20% volume of the circulatory blood) was injected intravenously into rats from the tail vein. The concentration decays of PEG_{Mn}(HSA-FeP2) in the blood showed single exponentials with half-life [$\tau_{1/2}$(FeP2)] of 13−16 h (Figure 14c). These values are considerably longer than those of the corresponding nonmodified HSA-FeP1 (*168*). Surface modification of HSA-FeP2 by PEG prevented the rapid clearance of the incorporated FeP2. On the basis of these findings, we can conclude that surface modification of HSA-FeP2 by PEG comprehensively improved its O_2 transporting ability.

We then proceeded to evaluate physiological responses to an exchange transfusion with PEG_{M2}(HSA-FeP2) in an acute anemia rat model (*169*) (Figure 15). The animals were first placed in a 65 vol % hemodilution with 5 g/dL HSA. They subsequently underwent a 30 vol % blood replacement with the PEG_{M2}(HSA-FeP2) solution. As negative and positive control groups, a 5 g/dL HSA solution (HSA group) and washed RBC suspension (RBC group) were infused, respectively, to similarly operated rats in hemorrhage. The isovolemic 65% hemodilution with HSA reduced the Hb concentration, thereby decreasing the O_2 supply to the tissue. Consequently, the mean arterial pressure (MAP), renal cortical O_2 partial pressure [PtO_2(R)], and O_2 partial pressure of muscle tissue [PtO_2(M)] were decreased. During hemorrhagic shock by 30% bleeding, significant decreases in the MAP, venous O_2 pressure (PvO_2), PtO_2(R), and PtO_2(M) were observed by the loss of the circulation blood volume. The heart rate (HR) and respiration rate were also decreased. In contrast, arterial O_2 pressure (PaO_2) increased to about 160% of the basal value (b.v.). The arterial CO_2 pressure ($PaCO_2$) decreased to about 62% of the b.v.; the pH increased to 7.55.

The injection of the sample solutions increased the blood volume and improved the circulatory flow. Lactate was washed out from the tissues and into the circulatory system, which decreased the pH to the initial level of 7.43 in all groups. The administration of HSA restored no parameters: death occurred within 41 min. In contrast, the infusion of PEG_{M2}(HSA-FeP2) or RBC kept all the rats alive until the end of measurements. After injection of PEG_{M2}(HSA-FeP2), the animals showed marked and rapid recovery in MAP, HR, PaO_2, PvO_2, $PaCO_2$, and pH, resembling that shown in the RBC group. These results demonstrate the O_2 transporting capability of the PEG_{M2}(HSA-FeP2) solution as a resuscitative fluid. We observed that albumin-based oxygen carrier does not induce hypertensive action, because of its low permeability through the vascular endothelium in comparison with that of Hb molecules. The heart rate responses after the injection were also negligibly small. Visualization of the intestinal microcirculatory changes clearly revealed the widths of the venule and arteriole to be fairly constant (*170*).

Reversible oxygenation of PEG_{M2}(HSA-FeP2) was observed even in the solid state (*171*). The aqueous solution of PEG_{M2}(HSA-FeP2(CO)) complex was spread on the glass plate and dried overnight at room temperature, producing a red transparent solid membrane (Figure 16a). In contrast, HSA-FeP2 without PEG decollation yielded a brittle membrane with many cracks. Scanning electron microscopy (SEM) observations of the PEG_{M2}(HSA-FeP2) membrane showed a uniform thickness of 15 μm and a smooth surface (Figure 16b). The $\tau_{1/2}(O_2)$ was 40 h, which is three times longer than the value in water. The

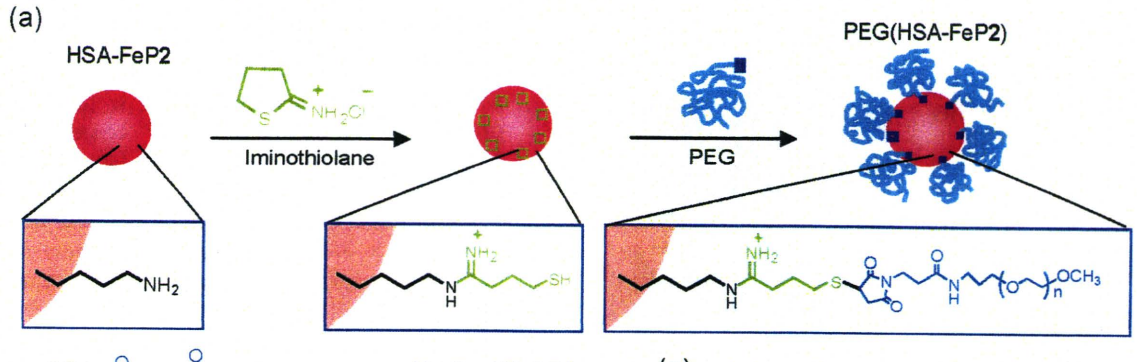

(b)

Solution and O_2 binding properties of PEG_{Mn}(HSA–FeP2)[a]

Samples	M_w of PEG	Viscosity (cP)	COP (Torr)	P_{50} (Torr)
PEG_{M2}(HSA–FeP2)	2 × 10³	1.14	27	32
PEG_{M5}(HSA–FeP2)	5 × 10³	2.34	65	31
HSA–FeP2	-	1.05	21	35

a) In phosphate buffered solution ([HSA]: 5g/dL, PEG_{Mn}/HSA–FeP2= 6, mol/mol) in average, pH 7.3, 37°C.

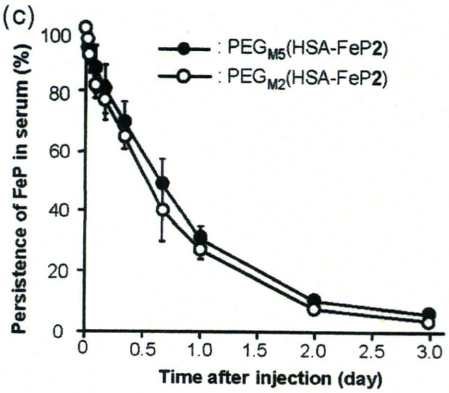

Figure 14. Surface modification of HSA-FeP with poly(ethylene glycol). (a) Synthetic scheme of PEG_{Mn}(HSA-FeP2). (b) Solution and O_2 binding properties. (c) Persistence of FeP2 in serum after administration of PEG_{Mn}(HSA-FeP2) into Wistar rats. Each value represents the mean ± SD of four rats.

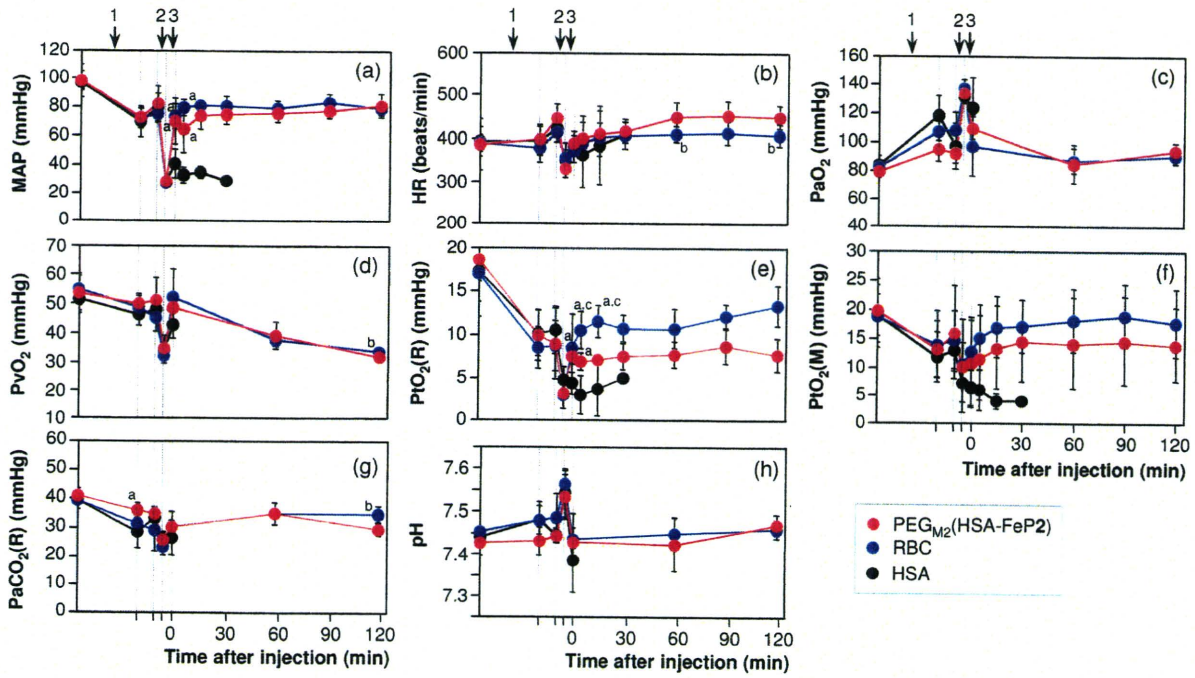

Figure 15. Effect of PEG_{M2}(HSA-FeP2) solutions on (a) MAP, (b) HR, (c) PaO_2, (d) PvO_2 (e) PtO_2(R), (f) PtO_2(M), (g) $PaCO_2$, and (h) pH in anesthetized rats subjected to hemodilution and hemorrhage. Each value represents the mean ± SD of five rats [red, PEG_{M2}(HSA-FeP2) group; blue, washed RBC group; and black, HSA group]. Arrows (1), (2), and (3), respectively, indicate the periods of 65% hemodilution, 30% bleeding, and sample infusion. [a] $p < 0.05$ versus HSA group (Tukey-Kramer test), [b] $p < 0.05$ versus PEG_{M2}(HSA-Fe2) group (unpaired *t*-test), and [c] $p < 0.05$ versus PEG_{M2}(HSA-FeP2) group (Tukey-Kramer test).

O_2 binding affinity was about a half that of the monomeric PEG_{M2}(HSA-FeP2).

We subsequently added hyaluronic acid (HA) as a supporting polymer to the protein solution and prepared the solid membrane on a poly(styrene) dish. Actually, HA is known as a glycosaminoglycan component of connective tissues, hyaline bodies, and extracellular matrix (*172*). Water evaporation of the PEG_{M2}(HSA-FeP2)/HA mixture ([HSA]: 2.5 wt % and [HA]: 0.2 wt %) produced a uniform red solid membrane that was easily peeled from the dish, yielding a free-standing homogeneous thin film of the PEG(HSA-FeP2)/HA hybrid (Figure 16c,d).

The PEG_{M2}(HSA-FeP2) solution is useful as a valuable O_2-carrying plasma. Membranes of PEG_{M2}(HSA-FeP2) with micrometer thickness can serve as a RBC substitute that can be preserved anywhere and reproduced as a saline solution at any time.

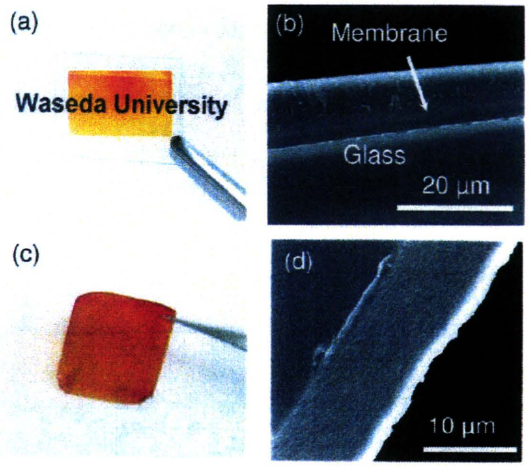

Figure 16. The solid membrane of PEG_{M2}(HSA-FeP). (a) Photograph of the membrane on the glass, (b) SEM of the membrane section, (c) photograph of the flexible film peeled from the poly(styrene) dish, and (d) SEM of the isolated film.

3.3. Recombinant HSA-Heme (rHSA-Heme) Prepared Using Site-Directed Mutagenesis. Hemin [Fe^{3+}protoporphyrin IX] released from metHb during enucleation of RBC or through hemolysis is captured by HSA with a high binding constant ($K \approx 10^8\ M^{-1}$) (*173*). Crystallographic studies have revealed that hemin is bound within a narrow D-shaped hydrophobic cavity in subdomain IB with axial coordination of Tyr-161 to the central ferric ion and electrostatic interactions between the porphyrin propionates and a triad of basic amino acid residues (Arg-114, His-146, and Lys-190) (Figure 17) (*174, 175*). In terms of the general hydrophobicity of this α-helical heme pocket, the subdomain IB of HSA potentially has similar features to the heme binding site of Hb or Mb. However, when one reduces HSA-hemin to obtain the ferrous complex, it is autoxidized rapidly by O_2, even at low temperature (~0 °C), because HSA lacks the proximal His, which, in Hb and Mb, enables the prosthetic heme group to bind O_2. Knowledge of the detailed architecture of the heme binding site in HSA enables us to design mutagenesis experiments to construct a tailor-made heme pocket for stable O_2 binding. Therefore, we used site-directed mutagenesis to introduce an His into the heme binding site that was expected to provide axial coordination to the central Fe^{2+} atom of the heme and thereby promote O_2 binding.

Results of our modeling experiments suggested that a favorable position for the axial imidazole insertion would be Ile-142 (Figure 17). The N_ϵ(His)-Fe distances were estimated as 2.31 Å for H142 (compared to 2.18 Å for Mb). We therefore designed and produced two single mutants I142H and a double mutant I142H/Y161L (HL) (*176*).

In the UV−vis absorption spectrum of rHSA(HL)-hemin, the ligand-to-metal charge transfer band at 625 nm was weakened because of the Y161L mutation. The MCD spectrum of rHSA(HL)-hemin showed a similar S-shaped pattern in the Soret band region resembling that of ferric Mb (*177, 178*). These results suggest that rHSA(HL)-hemin is in a predominantly ferric high-spin complex having a water molecule as the sixth ligand. The rHSA-hemin was easily reduced to the ferrous complex by adding a small molar excess of aqueous sodium dithionite under an Ar atmosphere (Figure 18). A single broad absorption band (λ_{max}: 559 nm) in the visible absorption spectrum and the MCD spectrum of rHSA(HL)-heme indicated the formation of a five-N-coordinate high-spin complex (*176, 177, 179*). The heme therefore appears to be accommodated in the mutated heme pocket with an axial coordination involving His-142. Upon exposure of rHSA(HL)-heme solution to O_2, the UV−vis absorption changed immediately to that of the O_2 adduct complex (Figure 18). It formed a carbonyl complex under a CO atmosphere. The single mutant rHSA(I142H)-heme, which retains Y161, was unable to bind O_2. The polar phenolate residue at the top of the porphyrin plane is likely to accelerate the proton-driven oxidation of the Fe^{2+} center. The replacement of Tyr-161 in rHSA(I142H)-heme by Leu enhanced stabilization of the O_2 adduct complex.

To evaluate the kinetics of O_2 and CO bindings to rHSA-hemes, laser flash photolysis experiments were carried out (Tables 7 and 8). It is noteworthy that the absorbance decay accompanying the CO recombination to rHSA(HL)-heme was composed of double-exponential profiles, which is normally not observed in Mb (the faster phase is defined as species I; the slower phase is defined as species II). The ratio of the amplitude of the species I and the species II was approximately 3:2. On the other hand, the rebinding of O_2 to rHSA(HL)-heme followed a simple monophasic decay. Numerous investigations of synthetic model hemes have helped to reveal the relation between the structure around the hemes and their O_2 and CO binding abilities (*4, 147, 148*). A bending strain in the proximal base coordination to the central Fe^{2+} atom, the "proximal-side steric (proximal pull) effect", is known to be capable of both increasing the dissociation rate for CO and decreasing the association rate. Simultaneously, it increases the O_2 dissociation rate without greatly altering the O_2 association kinetics. Consequently, one possible explanation for the existence of the two phases is that two different geometries of the axial His (His-142) coordination to the central ferrous ion of the heme might exist, each one accounting for a component of the biphasic kinetics of CO rebinding.

3.4. Modulation of O_2 Binding Property of rHSA-(mutant)−Heme. To control the O_2 binding affinity of rHSA-heme, we designed and produced diverse rHSA(mutant)−hemes in which bulky hydrophobic or hydrophilic amino acids were introduced around the O_2 binding site (Tyr-161, Leu-182, Leu-185, and Arg-186) (Figure 17). More recently, the beneficial effect of low-dose CO on the microcirculation by a hemoglobin-based artificial oxygen carrier has been discussed (*132, 182*). Control of the CO binding affinity of rHSA−heme is also tempting.

A. Substitution of Tyr-161 with Leu or Phe. The first, Tyr-161, was substituted to noncoordinating and hydrophobic amino acids (Leu or Phe). The O_2 and CO binding properties of rHSA(HL)−heme and rHSA(I142H/Y161F)−heme [rHSA(HF)−heme] showed that the presence of a Phe rather than a Leu at position 161 results in 6-fold and 4-fold increases in the O_2 binding affinity for species I and II, respectively (Table 7). This enhancement is mainly attributable to an increase in the O_2 association rate constant. The same trend was observed for CO binding [3-fold increase in k_{on}(CO)] (Table 8). The substitution of Leu-161 (102 $Å^3$) by Phe-161 (137 $Å^3$) (*183*) replaces an isopropyl group with a rigid benzyl group within the heme pocket. In rHSA(HL), the small side chain of Leu-161 might enable free rotation of the side chain of neighboring Leu-185, thereby reducing the volume on the distal side of the porphyrin plane (Figure 19a,b). On the other hand, the bulkier aromatic side chain of Phe-161 might prevent rotation of the isopropyl group of Leu-185 and thereby provide greater room of the distal pocket; this effect might provide easier access to the heme Fe^{2+} atom and account for the increased association rates for O_2 and CO.

B. Substitution of Leu-185 with Polar Amino Acid. Leu-185 was substituted with a more hydrophilic amino acid (Asn, Gln, or His), which was expected to interact with the coordinated O_2 by hydrogen bond and to stabilize the O_2 adduct complex similarly to Hb and Mb. In rHSA(mutant)−hemes in which Gln or His was introduced into Leu-185, they formed ferrous six-coordinated low-spin complexes under an Ar atmosphere. That

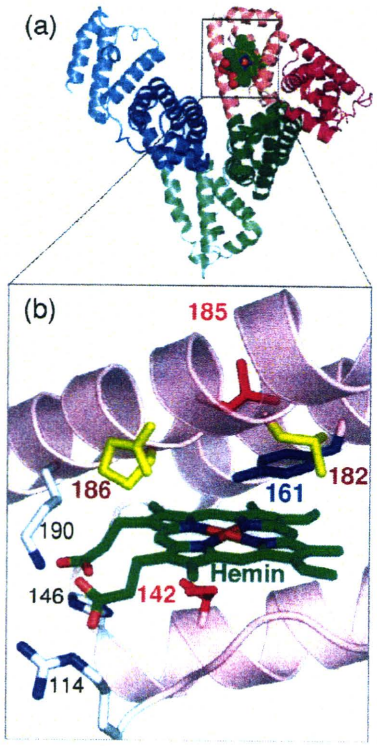

rHSA–heme	Position				
	142	161	182	185	186
Wild type	Ile	Tyr	Leu	Leu	Arg
I142H	***His***	Tyr	Leu	Leu	Arg
I142H/Y161L (HL)	***His***	***Leu***	Leu	Leu	Arg
I142H/Y161F (HF)	***His***	***Phe***	Leu	Leu	Arg
HL/L185N	***His***	***Leu***	Leu	***Asn***	Arg
HF/L185N	***His***	***Phe***	Leu	***Asn***	Arg
HL/L185Q	***His***	***Leu***	Leu	***Gln***	Arg
HF/L185Q	***His***	***Phe***	Leu	***Gln***	Arg
HF/L185H	***His***	***Phe***	Leu	***His***	Arg
HL/R186L	***His***	***Leu***	Leu	Leu	***Leu***
HL/R186F	***His***	***Leu***	Leu	Leu	***Phe***

Figure 17. (a) Crystal structure of HSA-hemin complex (1O9X) from ref 174. Hemin is shown in a space-filling representation. (b) Heme pocket structure in subdomain IB and positions of amino acids where site-specific mutations were introduced. Abbreviations of rHSA(mutant)s are shown in the table.

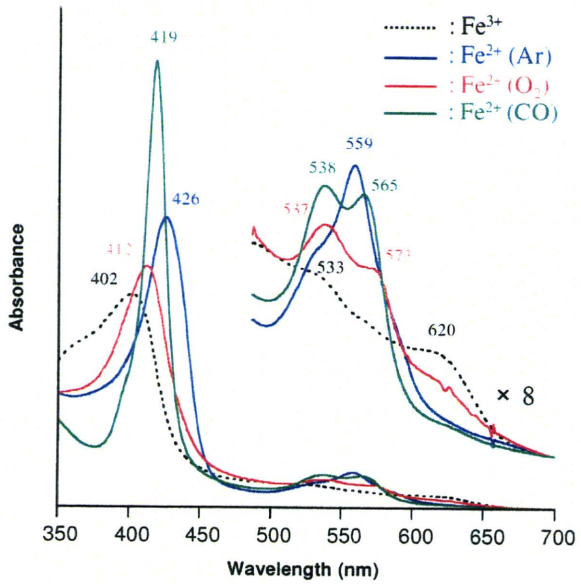

Figure 18. UV−vis absorption spectral changes of rHSA(HL)-heme in potassium phosphate buffered solution (pH 7.0).

result suggests that the introduced amino acid coordinates to the heme iron as a sixth ligand under an Ar atmosphere. Upon exposure of the solutions to O_2, they were oxidized. Bis-histidyl hemochromes are known to be oxidized by O_2 rapidly via an outer sphere mechanism (*184*−*186*). On the other hand, rHSA(HL/L185N)−heme and rHSA(HF/L185N)−heme in which Asn was introduced at Leu-185 formed ferrous five-coordinated high-spin complexes under an Ar atmosphere. They formed O_2 adduct complexes under O_2 atmosphere. The introduced Asn is estimated to be too far to coordinate to the heme.

Marked differences were apparent in a comparison of the O_2 and CO binding parameters for rHSA(HL)−heme and rHSA(HL/L185N)−heme. First, the presence of Asn rather than Leu at position 185 caused 2-fold and 3−6-fold increases, respectively, in the $k_{on}(O_2)$ and $k_{on}(CO)$ values. The Asn might partly rotate upward, which provides somewhat greater space of the distal pocket. Second, Asn-185 induced 18-fold and 10-fold increases in the O_2 binding affinity for species I and II, because the $k_{off}(O_2)$

Table 7. O_2 Binding Parameters of rHSA(Mutant)-Heme Complexes in Phosphate Buffered Solution (pH 7.0) at 22 °C

hemoproteins	$k_{on}(O_2)$ ($\mu M^{-1} s^{-1}$)	$k_{off}(O_2)$ ($m\ s^{-1}$)		$P_{50}(O_2)$ (Torr)	
		I	II	I	II
rHSA(HL)-heme	7.5	0.22	1.70	18	134
rHSA(HF)-heme	20	0.10	0.99	3	31
rHSA(HL/L185N)-heme	14	0.02	0.29	1	14
rHSA(HF/L185N)-heme	26	0.10	1.03	2	24
rHSA(HL/R186L)-heme	25	0.41	8.59	10	209
rHSA(HL/R186F)-heme	21	0.29	7.01	9	203
Mb[a]	14	0.012		0.51	
RBC[b]				8	

[a] Sperm whale myoglobin in 0.1 M potassium phosphate buffer (pH 7.0, 20 °C); ref 180. [b] Human red cell suspension in isotonic buffer (pH 7.4, 20 °C); ref 181.

Table 8. CO Binding Parameters of rHSA(Mutant)-Heme Complexes in Phosphate Buffered Solution (pH 7.0) at 22 °C

hemoproteins	$k_{on}(CO)$ ($\mu M^{-1}\ s^{-1}$)		$k_{off}(CO)$ (s^{-1})		$P_{50}(CO)$ (Torr)	
	I	II	I	II	I	II
rHSA(HL)-heme	2.0	0.27	0.013	0.079	0.0053	0.240
rHSA(HF)-heme	6.8	0.72	0.009	0.061	0.0011	0.068
rHSA(HL/L185N)-heme	6.8	1.60	0.008	0.039	0.0010	0.020
rHSA(HF/L185N)-heme	7.7	1.09	0.008	0.043	0.0008	0.032
rHSA(HL/R186L)-heme	5.0	0.57	0.011	0.165	0.0018	0.234
rHSA(HL/R186F)-heme	7.9	1.12	0.010	0.148	0.0010	0.107
Mb[a]	0.51		0.019		0.03	

[a] Sperm whale myoglobin in 0.1 M potassium phosphate buffer (pH 7.0, 20 °C); ref 180.